

Article

The Optimal Size of a Heterogeneous Air Taxi Fleet in Advanced Air Mobility: A Traffic Demand and Flight Scheduling Approach

Martin Lindner ^{*,†} , Robert Brühl [†], Marco Berger and Hartmut Fricke 

Institute of Logistics and Aviation, Technical University of Dresden, Hettnerstr. 1-3, 01069 Dresden, Germany; robert.bruehl@tu-dresden.de (R.B.); marco.berger@tu-dresden.de (M.B.); hartmut.fricke@tu-dresden.de (H.F.)

* Correspondence: martin_lindner@tu-dresden.de

† These authors contributed equally to this work.

Abstract: Introducing Advanced Air Mobility (AAM) as a novel transportation mode poses unique challenges due to limited practical and empirical data. One of these challenges involves accurately estimating future passenger demand and the required number of air taxis, given uncertainties in modal shift dynamics, induced traffic patterns, and long-term price elasticity. In our study, we use mobility data obtained from a Dresden traffic survey and modal shift rates to estimate the demand for AAM air taxi operations for this regional use case. We organize these operations into an air taxi rotation schedule using a Mixed Integer Linear Programming (MILP) optimization model and set a tolerance for slight deviations from the requested arrival times for higher productivity. The resulting schedule aids in determining the AAM fleet size while accounting for flight performance, energy consumption, and battery charging requirements tailored to three distinct types of air taxi fleets. According to our case study, the methodology produces feasible and high-quality air taxi flight rotations within an efficient computational time of 1.5 h. The approach provides extensive insights into air taxi utilization, charging durations at various locations, and assists in fleet planning that adapts to varying, potentially uncertain, traffic demands. Our findings reveal an average productivity of 12 trips per day per air taxi, covering distances from 13 to 99 km. These outcomes contribute to a sustainable, business-focused implementation of AAM while highlighting the interaction between operational parameters and overall system performance and contributing to vertiport capacity considerations.

Keywords: advanced air mobility; traffic demand; mobility data; flight scheduling; MILP optimization; productivity; delay management; battery charging; air taxi; eVTOL



Citation: Lindner, M.; Brühl, R.; Berger, M.; Fricke, H. The Optimal Size of a Heterogeneous Air Taxi Fleet in Advanced Air Mobility: A Traffic Demand and Flight Scheduling Approach. *Future Transp.* **2024**, *4*, 174–214. <https://doi.org/10.3390/futuretransp4010010>

Academic Editors: Panagiotis Georgakis, Babis Magoutas, Michiel de Bok, Suresh H. Renukappa and Subashini Suresh

Received: 15 December 2023

Revised: 11 January 2024

Accepted: 25 January 2024

Published: 11 February 2024



Copyright: © 2024 by the authors. Licensee MDPI, Basel, Switzerland. This article is an open access article distributed under the terms and conditions of the Creative Commons Attribution (CC BY) license (<https://creativecommons.org/licenses/by/4.0/>).

1. Introduction

Advanced Air Mobility (AAM) integrates urban and regional air transportation systems, and is expected to play a significant role in future mobility systems. By utilizing the third dimension, AAM can offer faster transportation using direct connections over longer distances while enhancing accessibility over competing transport modes due to very limited infrastructure-related requirements. Technological advancements, such as electric or hybrid engines and autonomous air taxis (also called eVTOLs), may further contribute to the acceptance and cost-effectiveness of air transportation.

However, the integration of AAM into existing transportation systems introduces several challenges:

- The complexity of the design of air taxis, involving modern battery resp. fuel cell technology and charging management within very limited space, including certification aspects;
- Airspace management in (congested) urban environments requiring advanced technologies to overcome safety concerns;
- Infrastructure development, such as the construction of landing and takeoff areas and charging stations ('vertiports') in potentially downtown urban areas with significantly limited space;

- Regulatory and legal challenges pertaining to air traffic management, privacy, environmental impact, and noise abatement;
- Concerns related to a potential societal shift, requiring coordination and cooperation among various stakeholders.

In Europe, various cities are part of the Urban Air Mobility Initiative Cities Community (UIC2), an initiative of the European Commission (EC) as an integral component of its Smart Cities Marketplace [1,2]. The primary objective of the UIC2 is to facilitate collaboration among cities actively implementing AAM, fostering knowledge-sharing and mutual support. Figure 1 visually depicts the locations of these cities and regions, marked by orange points [3]. Each region within the UIC2 framework possesses a distinct focus on AAM applications, with priorities ranging from logistics and medical services to artificial intelligence [4]. The Saxon government's exploration of AAM diverges from UIC2, focusing on rural areas with limited transportation infrastructure, rather than integrating AAM into already well-connected urban transit systems. Its primary aim is to advance these regions technologically and socially through AAM. Consequently, Dresden, the capital of Saxony and not a part of UIC2, is represented as a green point in Figure 1.



Figure 1. Map of European cities and regions participating in the UIC2 initiative for the implementation of AAM.

The successful integration of AAM depends on accurately determining the required fleet size of air taxis needed to match the projected demand within an anticipated operational framework. However, predicting this demand poses a challenge due to uncertainties surrounding the public acceptance of this novel mode of transportation and the dynamic nature of urban travel demands, which is currently still not foreseeable. Furthermore, the absence of a standardized model to evaluate fleet size, considering factors, like air taxi flight characteristics, existing transportation infrastructure, traffic regulations, population density, and pricing strategies, compound this challenge. The complexities are further compounded when examining rural areas, which exhibit distinct traffic dynamics, limited infrastructure, and unique economic considerations. Given the novelty of the AAM concept and the numerous questions, there are currently few approaches for developing an AAM network (cf. Section 2. Current approaches to fleet size determination predominantly rely on traffic simulations incorporating air taxis as an additional transport mode or traditional methodologies such as ongoing updates based on current bookings and forecasts, typically in commercial aviation fleet planning.

This study aims to address the research questions arising from the aforementioned constraints, aiming to bridge several gaps in the field. Firstly, it seeks to develop methodologies that translate mobility survey data into temporally and spatially resolved demand forecasts for AAM. Secondly, it aims to determine the optimal fleet size required to serve specific rural areas based on passenger demand and travel patterns. Thirdly, it investigates the impact of varying fleet sizes on performance metrics like travel time, passenger wait time, and overall system efficiency. This will provide valuable insights for efficient AAM, helping inform policymakers and stakeholders on the best strategies for implementing air taxi services. We assume that the necessary infrastructure and technology for AAM is available and there are no relevant regulatory constraints for scheduling and offering flights.

This paper is structured as follows: Section 2 provides an overview of demand modeling and a state-of-the-art on AAM technologies. Additionally, we explore the literature on capacity evaluation and the modeling of the number of required air taxis, considering different demand assumptions. Section 3 introduces the methodology for translating mobility data into forecasts for AAM demand. This section outlines the air taxi demand estimation approach from [5], which evaluates a segment of potential air taxi users and includes comprehensive calculations for air taxi flight performance. Section 4 presents the estimation of the number of air taxis required for AAM through a Mixed-Integer Linear Programming (MILP) model. This kind of vehicle and resource planning involves integrating flight scheduling, air taxi assignment, flight repositioning strategies, and considers additional waiting times due to battery charging during operations. Section 5 identifies the parameters for flight performance of each air taxi category to calculate estimated flight times and energy consumption. The comprehensive results are generated and presented in Section 6, followed by a thorough discussion in Section 7 within a broader context.

2. State-of-the-Art

2.1. Demand Forecast Modeling

Traffic demand forecast models synthesize the decision-making process of people in terms of mobility behavior. Thereby, people's decisions are influenced by their socio-demographic attributes (such as age, status of employment, and income), spatial characteristics (e.g., topography, urban or rural), and the offered mobility options (variety of transport modes, costs, and routes). To correctly model these decisions, the underlying parameters can be determined by calibrating a traffic model to meet an observed, empirical state. Traffic models usually consist of links and nodes with different relationships, capacities, or other restraints and of agents, as well as types of vehicles [6,7]. Furthermore, the demand patterns within various homogeneous groups in terms of travel behavior are derived from mobility surveys in Germany, such as System repräsentativer Verkehrsbefragungen (SrV) and Mobilität in Deutschland (MiD) [8,9]. A well-calibrated model allows statements to be made about future situations when changing some of the input variables. Thereby, urban transport modes are usually categorized into motorized and unmotorized individual traffic and public transport with different transport modes and vehicle types. This triggers people's decision to choose between mobility options. Most of the traffic results from mandatory activities such as work, education, and accompanying persons. Hence, daily traffic volumes follow fluctuations with usually one peak in the morning hours and one during the afternoon, which are mainly driven by these mandatory trips [7,10,11].

Predicting the impact of a new mode of transport on existing and potentially induced transport demand is challenging. The acceptance of new technologies and socio-economic developments create systematic interactions that cannot be predicted without further analysis [12]. Conventional transport demand forecast models, which rely on individual traffic patterns, personal attitudes towards different modes of transport, and specific data, cannot be applied easily to AAM, since historical data are missing.

In [13], an overview of scientific research concerning AAM, demand forecast modeling is given. Most of these estimate the AAM demand for specific regions to design a suitable network. The regions are the USA [14,15] (New York [16], Tampa [17], San Fran-

cisco [18–20]), Asia (Seoul [21,22]), and Europe (Paris [20], Munich [20,23,24], Zurich [25]). Most of these regions can be characterized by smaller areas with a high population density to overcome the crowded transport situation on the ground. In this work, we address an extensive region with lower population density to enhance the public transport situation, particularly in rural areas of the region where public transport is not sufficient. For this, our case study Saxony has mostly the same modal characteristics as regular regional- or longer-distance public transport. Travelers enter the air taxi on a designated spot located centrally and exit the AAM network on such a spot at the destination. As for that, not only the regional but also local accessibility ('the last mile') matters.

To address the AAM demand estimation challenge, the Airport Cologne/Bonn (CGN) estimates the potential demand for air taxis by calculating modal shift rates based on mode characteristics by using its own modal split data for passenger arrivals at the airport [26]. The assumption is that initial air taxi users will come from existing modes of transport without considering induced traffic demand. However, increasing the speed of travel between two locations can lead to primary induced traffic, which generates new demand. This can also lead to new spatial–structural and economic equilibrium states, possibly resulting in further (induced) traffic [27]. The concept of modal shifting is not new, and has been formerly discussed from private cars to public transport as a means of reducing emissions [28]. Here, the authors introduce attractiveness characteristics for making public transport a valuable option, such as costs (pricing), safety/security, comfort, information, travel frequencies and times, and ease of use [28]. Since this contribution is focused on how AAM can improve the existing transport system intelligently without replacing current modes of transport, it is assumed that AAM must also possess these characteristics to be appealing to the population. The approach of modal shifting in the context of AAM demand modeling only requires data from mobility surveys and population figures, which are often publicly available. The intent behind this is to identify travel patterns and connections with a high demand, for which AAM could be suitable in the future. The advantage of this approach is that it can be transferred to any region of interest.

However, it is important to note that the demand for AAM may change as the technology evolves, and continuous monitoring and analysis of travel patterns and user preferences will be necessary to accurately determine the demand. In this contribution, the demand modeling only concentrates on the modal shift of individuals and does not include potential induced traffic demand (see Section 3). Furthermore, it is assumed that there is social acceptance of AAM (according to a former acceptance study in the use case region, see [29]), respective political and operational regulations, appropriate ground infrastructure, and air equipment.

2.2. Operational Aspects of Air Taxis

2.2.1. Air Taxi Categories

Air taxis can be categorized into three groups based on their construction (fixed and/or rotary wings) and lift/thrust production during horizontal flight segments: *Vectored Thrust*, *Lift and Cruise*, and *Multicopter* [30–34]. These categories use electrical energy for propulsion [35], but are supposed to differ in terms of operational characteristics such as range, flight speed, and passenger capacity. As per [36], the battery mass is assumed to be around one-third of the Maximum Take-Off Mass (MTOM). The air taxi range depends on the specific energy density of the battery, which typically ranges between 200 and 250 Wh kg⁻¹ [33,37,38]. For the first generation vehicles, the passenger capacity (payload) will be limited to one to seven passengers assuming 100 kg mass per passenger including luggage [31].

In cruise, the *Vectored Thrust* and *Lift and Cruise* concepts behave similarly to conventional fixed-wing aircraft. However, for climb and descent, *Vectored Thrust* concepts have tilting elements that allow propulsion engines to be adjusted in the desired direction, while *Lift and Cruise* concepts hold independent systems. *Multicopter* concepts are similar to conventional helicopters with multiple horizontally mounted rotors and have high energy

efficiency in vertical flight segments. These air taxi categories can each be assigned to specific routes within a network based on their estimated flight ranges, passenger capacities, and energy consumption following pre-set optimization criteria [31].

2.2.2. AAM Flight Mission Profile

A generalized flight mission profile of an AAM air taxi operation is based on the International Civil Aviation Organization (ICAO) DOC 8168 [39], where traditional aircraft missions are divided into take-off, climb, cruise, descent, and (missed) approach segments. In [40], these segments are also considered for AAM. This approach is extended for AAM in previous studies [40,41], incorporating taxi segments before take-off and after landing, as well as a transition phase for changing the configuration from vertical to horizontal, particularly necessary for *Vectored Thrust* and *Lift and Cruise* electrical vertical take-off and landing (eVTOL). In this study, the AAM flight mission profile includes taxi, vertical take-off, cruise, and vertical landing segments. An acceleration and deceleration phase is introduced before and after the cruise segment, where the air taxi accelerates to its cruise speed after vertical take-off and decelerates to zero before vertical landing (see Figure 2). This distinction is made for improved performance, energy, and time modeling purposes (refer to Section 5).

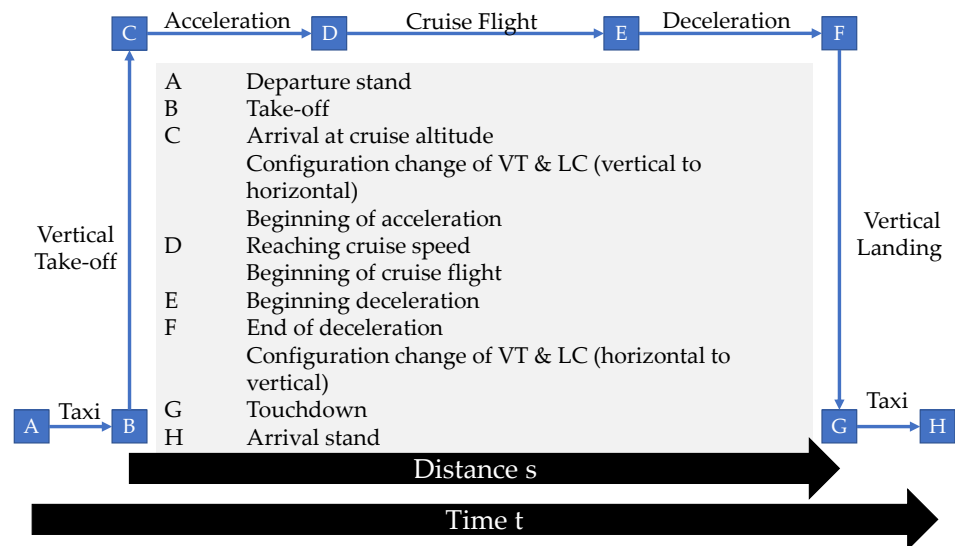


Figure 2. Generic flight mission profile for air taxi operations.

It is essential to note that this flight mission profile is a simplified representation, and the duration of the vertical takeoff depends on the obstacle situation at each vertiport. From an energy demand perspective, the presented profile represents the most demanding case due to the pure vertical climb without any forward flight movement. In the end, the certification process of each eVTOL aircraft type reveals the later operational mission profiles.

2.2.3. Turnaround Procedures

The battery capacity of air taxi is discussed in [31,42], where it is split into total and usable energy (80%), leading to a reserve of 20% to account for contingency procedures and potential re-routing. Depending on the distance to be covered and corresponding energy consumption, intermediate or inter-trip recharging at a destination is required, with this happening during the air taxi ground time, or turnaround. Recharging is identified as laying on the critical time path [42], representing the most time-consuming process during air taxi turnaround. Maintenance, Repair, and Overhaul (MRO) works during turnaround are only mentioned for the sake of completeness. Currently, there are no specific analyses regarding these tasks, e.g., cleaning the exterior.

Regardless of the specific designation used, it is assumed that the required infrastructure for air taxi operation (including all equipment, e.g., charging) is available in the use case network. Additionally, it is assumed that the air taxi categories are certified for passenger operation.

2.3. Vehicle Fleet Sizing Problems

Estimating the required number of vehicles to operate in a transportation network satisfying a given demand is well studied and defined as a Fleet Sizing Problem (FSP), e.g., for conventional aircraft fleets. Regression analysis is one of the commonly used methods to solve these problems by providing a quantitative estimate of the relationship between a dependent variable (the demand) and independent variables (the number of vehicles). In early research, Beamon and Chen [43] use regression methods to estimate fleet size in an industry system. They use different indicators to evaluate the production systems performance, where the most relevant measures for such problems are according to Imen et al. [44]: vehicle utilization rate, throughput rate, vehicle waiting time, vehicle blockage time, empty vehicle traveling time, total number of delivered loads or passengers, waiting time of units/passengers to be transported. All of them can be directly transferred to a specific transportation problem, such as the present one, and so also for AAM. Ehlers et al. [45] also demonstrated a further possibility for evaluating a mixed fleet based on an economic efficiency compared to other fleet compositions via a Fleet Efficiency Factor. Recent works based on regression methods are focusing on fleet sizing summarized under the term Mobility on Demand for shared bikes [46–49], cars and taxis [50–52]. Similarities can be found also for the optimum mix and size of air taxi fleets in the aviation industry [53–56].

However, regression analysis requires a sufficient sample size with the assumption of exogeneity of the independent variables. Often, historical demand and fleet data are analyzed as input data to identify patterns and trends and estimate the required fleet size. However, these databases do not exist for AAM. Here, potential future demand must be estimated using market research methods to determine the optimal fleet size and schedule [57]. Due to these disadvantages, regression analysis is barely able to capture the variability of demand due to seasonality and daily fluctuations, as well as fundamental uncertainty in determining demand. Especially, the future number of flights in the considered AAM network is uncertain because there is little knowledge about demand (general acceptance, comfort, pricing) as well as the operational constraints (range, speed, capacity, available in air time due to maintenance and battery charging times). In addition, typical fleets are composed of vehicles with different specifications in terms of range, capacity, and cost structures (both fixed and variable). By regression methods, the assignment of specific transport tasks to these vehicles is only possible by dividing the tasks into subgroups with similar characteristics.

To address these problems, different kinds of *simulations* are suitable. Agent-based simulations can model optimum fleet sizes by creating virtual agents that mimic the decision-making of vehicles, passengers, and other actors in a transportation system. This allows for complex system modeling and scenario testing. Agent-based simulations are already being used in research to calculate fleet sizes in various transportation networks. Sha and Srinivasan [58] present an agent-based model that considers the independent decision-making and interactions across different supply chain operations and demonstrate that fleet size significantly impacts the performance of the supply chain including customer satisfaction. By the probabilistic nature of freight transportation processes, Samchuk et al. [59] use simulation runs to investigate the service quality depending on the number of vehicles and assess the resulting truck utilization rate. A similar methodology is used by Valmiki et al. [60] and Saprykin et al. [61], who determine the optimal fleet size for automated vehicles or taxi fleets, respectively, based on achieving a targeted service quality. However, these studies have highlighted that larger and more complex problems in this domain require significant computational resources, and may present a challenge to implementation. Rajendran and Shulman [62] propose a simulation model to determine the number of air taxis required

to fulfill potential demand in New York City. Their simulation is based on a commercial tool, and includes a queue of customers for AAM, which are either serviced by available air taxis or disappear from the system unsatisfied after a long wait time. The approach is suitable for determining the number of air taxis with subsequent evaluation of service level, but does not yet allow for fleet heterogeneity.

Further models approach the problem of finding the optimal fleet composition through numerical and analytical approaches. Relevant according to the literature are *queuing models* and *optimization problems*. Queuing models are applied in various industries to improve queue system efficiency and customer satisfaction by analyzing arrival and service rates. Papier and Thonemann [63] present a M/M/c/c queuing model for fleet planning of a cargo rail company by developing a lost sales rate and a profit function to optimize the fleet size and structure. However, queuing models assume idealized conditions, such as infinite resources, constant arrival rates, and first-come-first-served service, so they are limited to their inability to fully capture the real-world conditions that impact fleet performance [64]. Recently, Amjath et al. [65] introduced a combination of a queuing model with a MILP to find the optimal fleet sizing of trucks, but do not consider a heterogeneous fleet and stochastic features.

The MILP form is most commonly used for determining the optimal fleet size, and is solved either exactly or approximately using heuristics [66]. Vis et al. [67] introduce a problem minimizing the vehicle fleet size required for the transportation of containers in a terminal within a specific time window. The authors validate their estimates using a simulation, showing the effectiveness of the analytical model in the context of a container terminal. Li and Tao [68] expand upon these concepts to include vehicle repositioning between two cities to meet the demand of a rental company and calculate an optimal fleet size for this purpose. These types of repositioning are critical in mobility-on-demand scenarios to ensure that vehicles are brought to customers while minimizing empty trips. Repoussis and Tarantilis [69] and Çağrı Koç et al. [70] integrate the fleet sizing problem with the routing of each individual vehicle through the Vehicle Routing Problem (VRP), thus providing detailed statistics on the usage of each vehicle. Accordingly, the utilization of all vehicles in a fleet can be maximized.

Due to the typical NP-hardness of the presented MILP models, they are unsuitable for large problems due to the increasing computational effort. Instead, the present problem can be spatially and timely divided into smaller sub-problems and solved selectively. If highly relevant features such as the demand imbalance between peak and off-peak are taken into account [71], forecasts can be made for the necessary fleet size of future transport modes. If the properties and characteristics of the sub-problems' transport networks also represent the cross-section of the main problem, these forecasts can be used for upscaling to the main problem with uncertainties. Those uncertainties can then be determined, for example, via Monte Carlo Simulation (MCS) to specify the required fleet size more precisely. By combining these methods, an approach for determining fleet sizes can be provided, even if the boundary conditions are still relatively uncertain at the current time.

3. Case Study and Air Taxi Flight Performance

This section introduces the network of the case study and outlines key assumptions related to demand estimation, air taxis, and flight planning. These assumptions form the foundational framework for addressing the primary research questions in the subsequent analysis.

3.1. Case Study, Network and Demand for Trips

The traffic network of the case study in this work is a result of preliminary work during the 'SmartFly' research project [5] and shown in Figure 3. It depicts a hub-and-spoke air taxi network in Saxony, with Dresden serving as the central hub. The network design is based on German mobility data (SrV [8,72] and MiD [9]) that has been evaluated for sketching the daily ground-based commuting situation around Dresden [73]. The combined data of

SrV and MiD is structured into three levels: households, individuals, and trips. In sum, there are listed 157,000 households with approximately 320,000 individuals living in there, resulting in around 971,000 single trips. Each household has a unique code to which the other levels are linked so that each resulting trip can be assigned to any individual in the household. The trip data are filtered to the region of Dresden, resulting in approx. 1100 daily ground-based trips (each trip corresponds to one person) originating or terminating in Dresden. Under these circumstances, Table 1 summarizes the most frequently mentioned destinations with their total number of trips per destination, corresponding relative shares on the total ground-based trips, and the Great Circle Distance (GCD) between Dresden and the respective cities. All in all, this leads to the reduction from originally 1100 ground-based trips to 497 relevant ones (corresponds to 43.5% of the total ground-based trips) that are originating or terminating at Dresden, which serve as the basis for further analysis (see Section 3.2). The remaining 56.5% of the ground-based trips between other cities and rural regions are excluded in further analysis, as they only have a very small share of the total trips. Therefore, and at this stage of work, no significant demand for air taxi services is assumed for these locations.

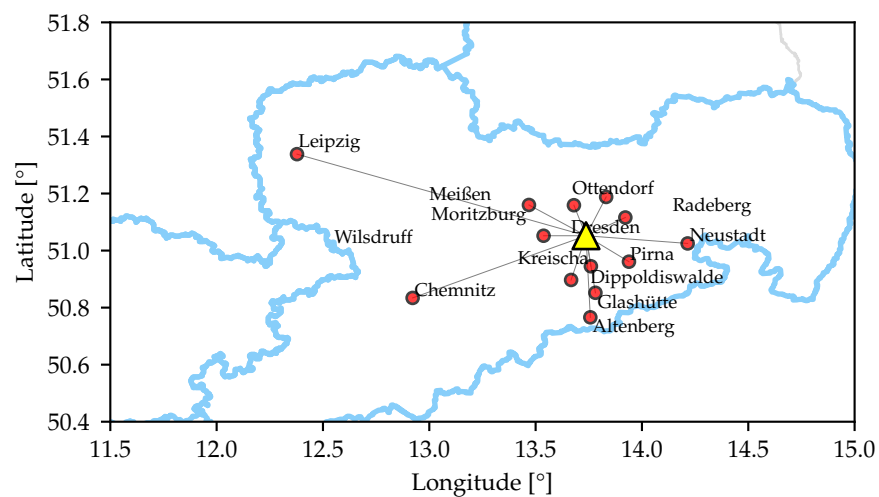


Figure 3. AAM network of the case study, connecting several cities in Saxony (red) with the network hub Dresden (yellow).

Table 1. Summarized SrV and MiD data for potential air taxi connections between Dresden and the surrounding areas in Saxony, including the total number of trips per destination and day, along with their corresponding relative shares in total ground-based trips and distance.

City	# Trips	Rel. Share [%]	GCD [km]
Pirna	103	9.0	17.4
Radeberg	77	6.7	14.8
Meißen	46	4.0	22.3
Glashütte	46	4.0	22.4
Wilsdruff	38	3.3	13.9
Ottendorf-Okrilla	32	2.8	16.5
Leipzig	29	2.6	99.9
Altenberg	27	2.4	31.8
Kreischa	22	1.9	11.9
Moritzburg	22	1.9	12.6
Dippoldiswalde	20	1.8	17.9
Neustadt in Sachsen	18	1.6	33.5
Chemnitz	17	1.5	62.1
Total	497	43.5	-

The network design itself is based on a linear cost optimization, where the model is developed in [74] and adjusted according to the characteristics of a pure hub-and-spoke network. The mobility dataset of SrV and MiD serves as a basis for the demand estimation, which is detailed in the subsequent Section 3.2. The aircraft rotation scheduling model in Section 4.1 also supports flights between non-hub cities, if required.

3.2. Air Taxi Travel Demand

In this section, the key assumptions underlying the demand estimation approach, including the proposed methodology based on modal shift rates, are highlighted.

The modal shift rates encompass considerations of established modes of transport and, conversely, aspects of social acceptance. This incorporates personal attitudes towards air taxis and includes statements about a potential intention to use them. In [29], aspects of social acceptance are surveyed within the Dresden use case region.

To measure the intention to use air taxis, three scenarios are introduced: longer distances for non-everyday occasions, individual routes from respondents' homes to Dresden city center, and network commuting in alignment with a public transport system. For the presented use case network in this contribution, the focus is on network commuting, where a total of 21.6% of respondents stated that they would 'likely' use an air taxi in this context, at least to some extent (respondents could choose between one (not likely at all) and five (very likely)) [29].

Regarding mode-specific characteristics, the following assumptions, which also take financial aspects into account [74], are established:

- Bicycle trips typically involve shorter distances, characterized by very low financial outlay (purchase and maintenance costs for a bicycle). In this context, the motivation for using an air taxi could be driven by factors such as the fun factor or personal interests in technology [29].
- Public transport generally serves medium to long distances and travel times. Users in this category typically exhibit high price sensitivity, accepting longer travel times for a lower price compared to individual transport options. Here, the fun factor and potential technology interests could be influential in choosing an air taxi for sporadic trips.
- Trips covered by individual transport (e.g., cars) are also characterized by medium to long distances, resulting in a moderate willingness to pay. Users in this category accept higher operating costs for a car (purchase, fuel, maintenance, insurance) in exchange for time savings and individuality compared to public transport.

These assumptions suggest that individual mobility users are more likely to transition to air taxis than users from other modes [75,76]. Additionally, the purpose of the trip could play a significant role in terms of punctuality, especially for business reasons, and potential time savings [76–78]. Therefore, the assumed shifting rates from ground-based transport options to air taxis are as follows [74]:

- Car users: 15%.
- Public transport users: 5%.
- Bicycle users: 2%.

Now, these rates have to be extended by the previously described social acceptance (by multiplication with 21.6%), as they only consider the mode-specific characteristics at this point. Finally, the assumed mode-specific shifting rates are displayed in Table 2 [74].

Table 2. Mode-specific shifting rates [%] to AAM (modal shift and acceptance).

Bicycle	Car	Public Transport	Total
0.43	3.24	1.08	4.75

It should be noted that the estimation is subject to uncertainties, primarily due to the absence of air taxis in the current transport system. The calculation heavily relies on various assumptions that cannot be empirically validated at this stage. The estimated shifting rates, obtained from the mobility data (refer to Section 3.1), serve as the basis for the subsequent demand estimation.

The number of inhabitants for each prospective destination (refer to Table 1) is sourced from [79]. Subsequently, the relative shares per destination are utilized to extrapolate the sample findings of the mobility data evaluation to encompass the entire population of the respective cities. The identification of potential air taxi users is outlined in Table 3.

The population for each potential destination (refer to Table 1) is extracted from [79]. Following this, the relative shares per destination are employed to extrapolate the sample results from the mobility data evaluation, providing a comprehensive representation of the entire population of the respective cities. The estimated demand of potential air taxi users is presented in Table 3.

Table 3. Estimated demand for air taxi users ('AAM') based on mobility data. In total, 619 individuals are assumed to travel with AAM on a daily basis in the current network ('Total').

City	# Indv.	Car			Public Transport			Bicycle			AAM
		rel.	abs.	AAM	rel.	abs.	AAM	rel.	abs.	AAM	Total
Pirna	3481	0.73	2534	82.1	0.20	709	7.7	0.07	236	1.0	91
Radeberg	1266	0.70	887	28.8	0.25	312	3.4	0.05	65	0.3	32
Meißen	1141	0.63	719	23.3	0.30	347	3.7	0.07	74	0.3	27
Glashütte	268	0.93	250	8.1	0.07	17	0.2	0	0	0	8
Wilsdruff	480	0.84	404	13.1	0.16	75	0.8	0	0	0	14
Ottend./Okr.	280	0.94	262	8.5	0	0	0	0.06	17	0.1	9
Leipzig	15,309	0.48	7390	239.5	0.52	7918	85.5	0	0	0	325
Altenberg	190	1.00	190	6.2	0	0	0	0	0	0	6
Kreischa	87	0.91	79	2.6	0.09	7	0.1	0	0	0	3
Moritzburg	159	0.82	130	4.2	0.05	7	0.1	0.09	14	0.1	4
Dippoldisw.	254	0.80	203	6.6	0.20	50	0.6	0	0	0	7
Neustadt/S	189	0.89	168	5.5	0.11	21	0.2	0	0	0	6
Chemnitz	3695	0.59	2173	70.4	0.41	1521	16.4	0	0	0	87
619											

The first column in Table 3 corresponds to destinations connected with Dresden through AAM in this case study. The second column extrapolates the number of individuals traveling on each respective connection. For instance, Pirna has 38,681 inhabitants [79] and, by considering a relative share of nine percent derived from the mobility data (refer to Table 1), this results in 3481 individuals commuting between Dresden and Pirna, utilizing various modes of transportation. By using the modal split data provided in the mobility data (relative values per mode of transportation in Table 3), it becomes feasible to allocate the number of individuals (second column) to a specific mode of transportation (depicted as *absolute* values per mode of transportation in Table 3). The resultant count of individuals per mode of transportation is then multiplied by the previously estimated shifting rates (refer to Table 2), disclosing the number of individuals making the transition from the corresponding mode of transportation to an air taxi (AAM column per means of transportation). This process is executed for each destination, culminating in a total of AAM individuals shifting to air taxis daily (Pirna<->Dresden: 91 individuals per day). Moreover, Figure 4 provides a visual representation of this process using data from the Pirna–Dresden connection. It illustrates the extent of modal shift for each mode of transportation by depicting the mode-specific shifting rates outlined in Table 2. The direction of travel is not yet determined.

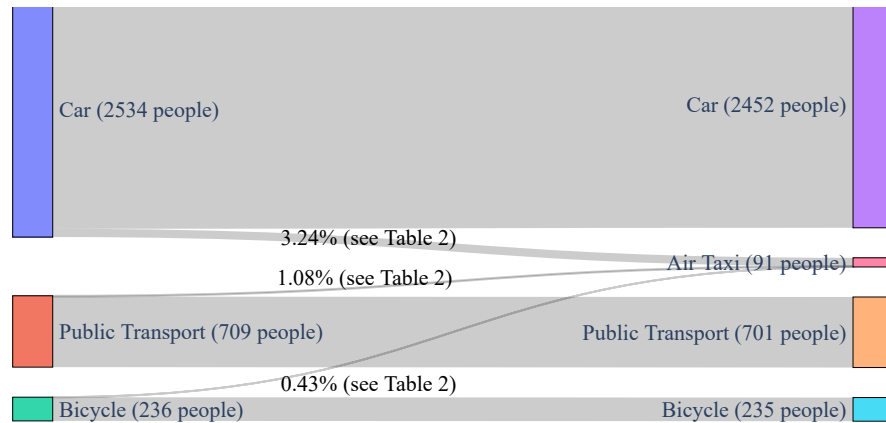


Figure 4. Modal distribution of travelers for the connection between Pirna and Dresden.

To address this challenge, it is assumed that the traffic demand is mainly driven by commuting activities. This is supported by [80], which provides such flows for specific regions in Germany. Particularly for commuters in Dresden, it reveals that 62% of commuters travel from suburban areas to Dresden and 38% of them from Dresden to suburban areas. This commuter behavior results in typical peak hours, as shown in Figure 5. The figure is approximated based on [72] and contains a distribution of all trips (all modes of transportation) in Dresden, represented by the black line (corresponding relative shares are summarized by Table A1). The other lines express the number of commuters traveling to Dresden (blue) and from Dresden (dashed blue). The green area shows the assumed operational time of air taxis, assumed to be from 6:00 a.m. to 10:00 p.m. due to a potential night flight restriction.

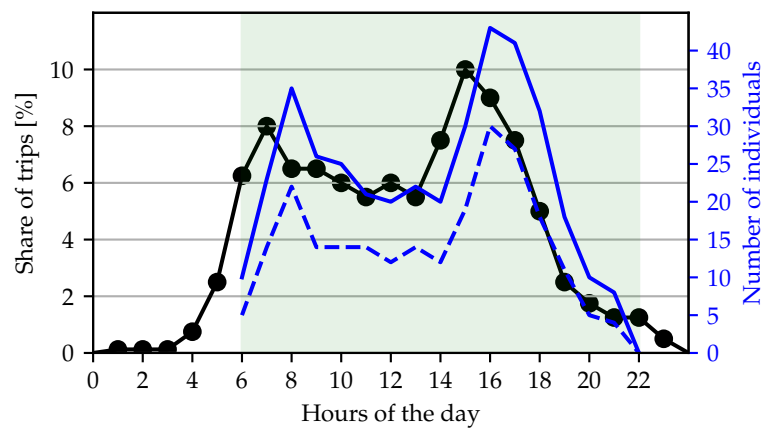


Figure 5. Share of total trips during the day (black, undirected, all means of transport) and number of individuals directed traveling to (blue, solid) and from Dresden per air taxi (blue, dashed).

Figure 6 illustrates the number of air taxi users according to their departures and destinations. Figure 6 left describes the distribution of individuals who are traveling to Dresden according to their departure locations and the time of the day, and Figure 6 right visualizes the equal context for the other direction of traveling (from Dresden to suburban areas). Both figures show the typical peak times during the day in the morning and afternoon hours. These time periods are the most significant ones for the determination of the required number of air taxis. In addition, the mission profile of AAM is also affecting the air taxi traffic flow. The mission profile (see Figure 2) includes the turnaround time, the flight time, and possible holding times, which altogether influence the possible utilization rate of an air taxi. If there is a schedule, such uncertainties can be reduced and delays can be minimized.

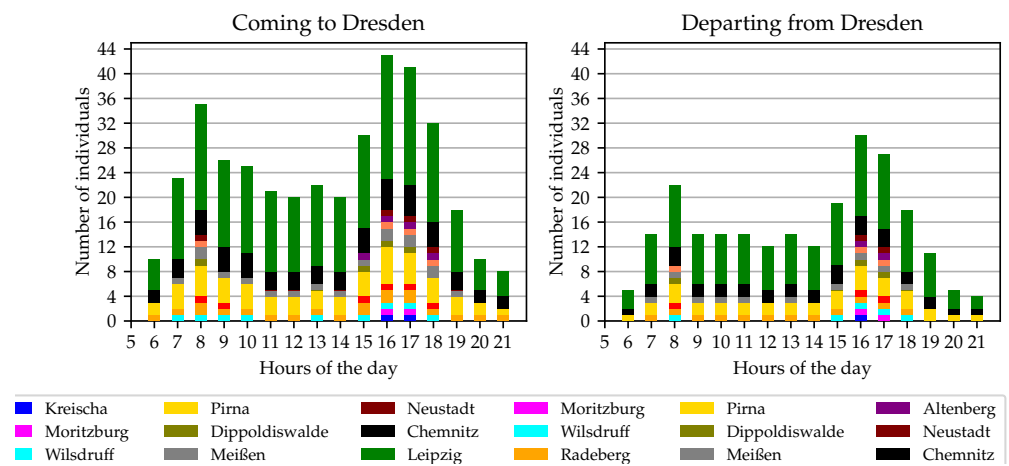


Figure 6. Number of air taxi users coming to and departing from Dresden, distributed by locations.

Given the impact of population size on demand, it is reasonable to anticipate a significant portion of air taxi travel demand between Leipzig and Dresden.

3.3. Air Taxi Flight Performance

Additional information regarding air taxis are essential for accurately determining the required fleet size, complementing the previously estimated demand potential for air taxi services (refer to Section 3.2). It is assumed that the air taxis are certified for passenger operation and authorized to fly, as detailed in Section 2.2. The GCD within the case study network ranges from 11.9 to 99.9 km. Table 4 summarizes all relevant data necessary for performance modeling, elaborated upon in the subsequent sections of this contribution. It should be noted that these values are idealized, as real flight conditions and the corresponding capabilities that the aircraft must demonstrate during the certification process remain unclear. Typically, performance modeling varies based on meteorological conditions (such as wind speed and direction, temperature, and air density) and equipment age.

Further details on air taxis are crucial for precise fleet size determination, supplementing the earlier assessed demand potential for air taxi services (see Section 3.2). It is presupposed that the air taxis are certified for passenger operations and possess the necessary flight authorization, as elaborated in Section 2.2. The GCD within the case study network ranges from 11.9 km to 99.9 km. All pertinent data essential for performance modeling is consolidated in Table 4, presented in the subsequent sections of this paper.

The range of the air taxi is limited by the characteristics of its battery (energy density E^*), which provides a specific amount of energy. As explained in Section 2.2, approximately one-third of the MTOM is attributed to the battery mass. The study conducted by [5] examines the MTOM of each air taxi category, as well as the payload (PL) of each aircraft, which contains a total of 22 air taxi (11 *Vectored Thrust*, eight *Lift and Cruise*, and four *Multicopter*). By multiplying the MTOM by 0.33, the battery mass can be determined, which can then be converted into a total amount of energy (E) by assuming an energy density of $E^* = 200 \text{ Wh kg}^{-1}$. The usable amount of energy (E_{use}) can be estimated using Equation (1), which takes into account a depth of discharge (DoD) of 0.8 to ensure that the reserve energy (20% of the total amount of energy) is available, as well as the introduction of a battery efficiency factor (η_{battery}) assumed to be 0.95 to account for heating losses in the battery.

$$E_{\text{use}} = E^* \cdot m_{\text{battery}} \cdot \eta_{\text{battery}} \cdot DoD \tag{1}$$

Table 4. Summarized parameters for air taxi performance modeling.

Parameter	Designation	Vect. Thrust	Lift and Cruise	Multicopter
Cruise speed	V_{cruise} [$m s^{-1}$]	72	40	24
Max. Take-Off Mass	$MTOM$ [kg]	2200	1600	900
Payload	PL [kg]	400	300	100
Battery mass	$m_{battery}$ [kg]	730	530	300
Battery mass ratio	$\frac{m_{battery}}{MTOM}$ [-]		0.33	
Energy density	E^* [$Wh kg^{-1}$]		200	
Total energy	E [kWh]	146	106	60
Battery efficiency	$\eta_{battery}$ [-]		0.95	
Depth of discharge	DoD [-]		0.8	
Efficiency during hover	η_{hover} [-]	0.70	0.75	0.8
Efficiency during cruise	η_{cruise} [-]	0.8	0.7	0.6
Efficiency during transition	η_{trans} [-]	0.65	0.7	-
Usable energy	E_{use} [kWh]	110.96	80.56	45.6
Disc Loading	DL [$N m^{-2}$]	1354.98	832.70	59.03
Air density	ρ [$kg m^{-3}$]		1.225	
Rotor rotation speed	v_h [$m s^{-1}$]	23.52	18.44	4.91
Rate of Climb	RoC [$m s^{-1}$]		5	
Tilt angle	Θ [$^\circ$]	82	90	-
Total disc area	A [m^2]	8	9.4	74.8
Wing surface	S [m^2]	11	11	-
Solidity	σ [-]	4.41	3.06	-
Rotor tip speed	V_{tip} [$m s^{-1}$]		187	
Drag coefficient	C_D [-]	0.039	0.061	0.098
Rotor drag coefficient	C_d [-]		0.0015	
Rotor diameter	d_{rotor} [m]	1.3	1.0	2.3
Number of rotors	n [-]	6	12	18
Number of blades per rotor	N [-]	5	2	2
Lift-to-Drag ratio cruise	$(\frac{L}{D})_{cruise}$ [-]	16	13	4

The performance modeling equations are presented in [31], based on [81–83], but used in this contribution with some modifications to account for the specific flight mission profile presented in Figure 2 (elimination of the horizontal climb segment). The final equations used to calculate the power requirements for each flight segment are briefly summarized in the subsequent sections.

3.3.1. Taxi

The taxi segments can be performed either as ground or hover taxi (GT and HT), depending on the availability of equipped landing gear. According to Patterson [84], the power requirement for a ground taxi (P_{GT}) can be estimated using Equation (2), and it depends on the power assumed for the cruise segment.

$$P_{GT} = 0.1 \cdot P_{cruise} \quad (2)$$

The power requirement for a HT (P_{HT}) depends on the disc loading (DL) (Equation (3)) and is estimated by Equation (4). For simplification, it is expressed as the power for a stationary hover flight (P_H).

$$DL = \frac{W}{A} = \frac{m \cdot g}{n_{rotor} \cdot 2\pi r_{rotor}^2} \quad (3)$$

$$P_{HT} = P_H = \frac{W}{\eta_{hover}} \cdot \sqrt{\frac{DL}{2\rho}} \quad (4)$$

3.3.2. Vertical Take-Off

The power for the vertical take-off (P_{TO}) depends on the power to hover (P_H), the rate of climb (RoC), and the rotor rotation speed (v_h) (Equation (5)).

$$P_{TO} = P_H \cdot \left[\frac{RoC}{2v_h} + \sqrt{\left(\frac{RoC}{2v_h}\right)^2 + 1} \right] \quad (5)$$

3.3.3. Transition

The transition segment is specific to *Vectored Thrust* and *Lift and Cruise* aircraft, as they necessitate a transformation from vertical to horizontal flight configurations in preparation for the subsequent horizontal phase after take-off (and vice versa before vertical landing). The power required for this transition, denoted as P_{Trans} , is expressed as the summation of three power components (as detailed in Equation (6)), where V_∞ represents the targeted velocity attained by the air taxi following the transition phase. Following Figure 2, it is assumed that the air taxi reaches its designated cruise altitude, executes the transition maneuver, and subsequently commences acceleration until the desired cruise speed is attained. Notably, the initial value of V_∞ is set to zero, signifying the air taxi's initiation of acceleration from a standstill (short stationary hover flight) to achieve its designated cruise speed.

$$P_{Trans} = P_{induced} + P_{drag, rotor} + P_{drag, aircraft} \quad (6)$$

$$P_{induced} = \frac{W}{\eta_{trans} \cdot \sin(\Theta_{tilt})} \cdot \sqrt{\frac{-V_\infty^2}{2} + \sqrt{\left(\frac{V_\infty^2}{2}\right)^2 + \left(\frac{W}{\sin(\Theta_{tilt}) \cdot 2\rho A}\right)^2}} \quad (7)$$

$$\sigma = \frac{\text{blade area}}{\text{rotor disc area}} = \frac{N \cdot c \cdot r_{rotor}}{\pi \cdot r_{rotor}^2} \cdot n = \frac{N \cdot c}{\pi \cdot r_{rotor}} \cdot n \quad (8)$$

$$P_{drag, rotor} = \rho A V_{tip}^3 \cdot \left(\frac{\sigma C_d}{8} \cdot (1 + 4.6\mu^2)\right) \quad (9)$$

$$P_{drag, aircraft} = 0.5\rho V_\infty^3 C_D S \quad (10)$$

3.3.4. Cruise

The power for the cruise (P_{cruise}) is the result of a lift and weight balancing by assuming that the drag equals thrust.

$$P_{\text{cruise}} = \frac{T \cdot V_{\text{cruise}}}{\eta_{\text{cruise}}} = \frac{W \cdot V_{\text{cruise}}}{\left(\frac{L}{D}\right)_{\text{cruise}} \cdot \eta_{\text{cruise}}} \quad (11)$$

3.3.5. Vertical Landing

The determination of power required for vertical landing (P_{VD}) follows a comparable methodology to that employed for vertical take-off, with the sole distinction being the consideration of a negative rate of climb (RoC).

$$P_{\text{VD}} = P_H \cdot \left[\frac{RoC_{\text{LD}}}{2v_h} + \sqrt{\left(\frac{RoC_{\text{LD}}}{2v_h}\right)^2 + 1} \right] \quad (12)$$

3.3.6. Energy Requirement

The energy consumption E_s of an air taxi depends on the power P_s and time t_s the vehicle spends in each flight segment s (Equation (13)).

$$E_s = P_s \cdot t_s \quad (13)$$

Assumed durations t_s per flight segment s are shown in Table 5. The duration for the vertical segments corresponds to a cruise altitude of 150 m and the RoC of 5 m s^{-1} (or -5 m s^{-1} in case of vertical landing). It has to be mentioned that the transition has to be performed twice (after vertical take-off and before vertical landing) for *Vectored Thrust* and *Lift and Cruise* air taxis with a duration of 20 s each.

Table 5. Assumed durations t_s per flight segment s .

Taxi	Vertical Take-Off	Transition	Vertical Landing
30 s	30 s	20 s	30 s

The duration of the cruise phase depends on the distance (GCD) between departure and destination minus the distance and time required for acceleration (from zero to cruise speed) and deceleration (from cruise speed to zero). Following the kinematics from Equations (14) and (15), the acceleration a is required.

$$s = \frac{v^2}{2a} \quad (14)$$

and

$$t = \frac{v}{a} \quad (15)$$

The acceleration data are from the Sophisticated Aircraft Performance Model (SOPHIA) for conventional small aircraft at the climb-acceleration phase [85]. Hereby, the mean acceleration value ($a = 2.2 \text{ m s}^{-2}$) is assumed for *Vectored Thrust* air taxi, $a = 1.54 \text{ m s}^{-2}$ for *Lift and Cruise* air taxi (70% of the mean), and $a = 1.1 \text{ m s}^{-2}$ for *Multicopter* (50% of the mean) (commonly used cars: 1.7 m s^{-2} up to 4.5 m s^{-2}). Deceleration values are chosen according to [86], where various values are determined for different aircraft at landing: *Vectored Thrust* $a = -0.6 \text{ m s}^{-2}$, *Lift and Cruise* $a = -0.5 \text{ m s}^{-2}$, and *Multicopter* $a = -0.4 \text{ m s}^{-2}$. The resulting values for distances and times for reaching the cruise speed (and zero in case of deceleration) are presented by Table 6. Practically, this means that the distances from Table 1 have to be reduced by the distances listed in Table 6 to obtain the remaining distance, on which aircraft travel with cruise speed.

Table 6. Resulting distances and times for corresponding acceleration and deceleration values per air taxi category.

Air Taxi Category	Cruise Speed [m s ⁻¹]	Acceleration		Deceleration	
		Distance [m]	Time [s]	Distance [m]	Time [s]
<i>Vectored Thrust</i>	72	1177	33	4320	120
<i>Lift and Cruise</i>	40	519	26	1600	80
<i>Multicopter</i>	24	262	22	720	60

The total amount of energy for the whole flight mission (E_{tot}) is expressed by Equation (16) by summing up the single energy requirements per flight segment s .

$$E_{\text{tot}} = \sum_{s=1}^n E_s = \sum_{s=1}^n P_s \cdot t_s \quad (16)$$

Additionally, it is important to note that the power requirements for each flight segment depend on the mass of the air taxi, necessitating the consideration of passengers as payload. For the subsequent performance modeling, the MTOM is taken into account.

3.3.7. Range

According to [87] the maximum range for electric flight can be estimated by using Equation (17), which depends on the energy density of the battery (E^*), the gravity g , the lift-to-drag ration ($\frac{L}{D}$), and the battery mass ratio (assumed with one third).

$$R = E^* \cdot \eta_{\text{tot}} \cdot \frac{1}{g} \cdot \frac{L}{D} \cdot \frac{m_{\text{battery}}}{m_{\text{aircraft}}} \quad (17)$$

Assuming an energy density of 200 Wh kg⁻¹ and a total system efficiency of 0.65 along the propulsion path, the computed results for maximum range per air taxi category are 250 km for *Vectored Thrust*, 200 km for *Lift and Cruise*, and 60 km for *Multicopter*. It is important to note that these ranges do not account for the energy consumption during the vertical segments. As a result, the anticipated maximum ranges are likely to be reduced, as demonstrated in Section 5.

4. Flight Scheduling and Aircraft Assignment Model

An optimization model for flight planning and scheduling is highly suitable for assessing air taxi productivity and daily utilization, aiding in determining the optimal aircraft count for a given schedule. Measuring productivity involves analyzing operational times from completed flights within the schedule, and addresses a Flight Scheduling Problem. Complexities like vertical take-off and landing impact productivity, managed effectively by the optimization model. This ensures efficient utilization and scheduling to meet diverse demands and enhance overall operational efficiency.

We define the problem as a modified version of the Heterogeneous Vehicle Routing Problem with Time Windows (HVRPTW), where each air taxi may possess distinct fleet properties and is assigned a route between time-window-constrained flights. Moreover, we introduce the concept of Soft Time Windows (STW) in terms of AAM, allowing for deviations from the intended scheduled departure times at added costs within the objective function. This empowers the solver to find a flight schedule that minimizes deviations from scheduled departure times based on traffic demand and enhances the management of air taxi utilization with greater flexibility.

The model has been previously presented by us in work on airline disruption management [88,89] and has now been adapted and extended to meet the requirements of AAM. We have omitted modeling of connecting passengers between flights and have opted for a less restrictive flight scheduling approach, allowing wider hard time window limits and

more intense use of accepted delay. Furthermore, the model includes repositioning and battery charging time calculation. The following constraints are additionally considered:

- Variables: flight schedule (departure and arrival times) with integrated air taxi allocation: which air taxi is assigned to which flight.
- Logical and valid flight schedule: no overlapping flights for an air taxi, sufficient turnaround time, time for repositioning, and a sufficient remaining battery energy level for the subsequent flight.
- Always sufficient available space at vertiports, along with immediately accessible and uninterrupted battery charging facilitated by the provided power supply. Upon arrival at the vertiport, passengers are ready for departure, thus no delays are anticipated.
- Route restrictions exist by air taxi range and capacity (refer later in the text to the corresponding parameters depicted in Figure 9).
- A standard ground time is estimated, which is used to prepare the aircraft for the flight and allows for passenger boarding and deboarding (later in text in Figure 10). This time can be utilized for battery charging.
- Reliable air taxis without failures; no maintenance units due to extended planning horizon, can be abstracted via allocated time slots per air taxi.
- No new incoming requests are allowed into the system; otherwise, the calculation must be restarted.

4.1. Mathematical Formulation

The model consists of a set of unique air taxis \mathcal{V} and a set of scheduled flights N including a dummy depot 0 representing the start and end of a route. The subset $C \subset N$ only includes flights and forms the directed graph $G = (V, C)$.

The set of ground arcs $A \subseteq N \times N$ contains the connections between flights. Each flight i has a flight duration F_{ik} , specific operating costs CN_{ik} and ground event costs CE_{ijk} for air taxi k (cf. Figure 7). A flight i is limited by a non-negative hard TW $[A_i, B_i]$, where A_i is the scheduled departure and B_i latest possible arrival time. The actual departure time s_i and arrival time e_i if the flight must lie within these limits. To allow for arrival delays, B_i should be set high to a problem-specific maximum acceptable delay duration.

An STW for flight i tolerates a deviation from the scheduled arrival time of this flight $SIBT_i$, but charges delays with costs in the objective function. The STW is described by the scheduled departure A_i and $SIBT_i$ in the interval $[A_i, SIBT_i]$. Thus, STWs start simultaneously with hard TWs, but are closed earlier ($SIBT_i \leq B_i$) to measure the delay from scheduled times. If the actual arrival time e_i of flight i exceeds $SIBT_i$, arrival delay occurs and is calculated by the variable d_i^{ARR} (cf. Figure 8).

A ground event has the duration of T_{ij} , consisting of a turnaround time and/or a repositioning flight, including additional specific turnaround time, if the destination of flight i is not equal to the departure of flight j . This value should always be parameterized to be sufficiently large to allow for a minimum ground time for air taxi pre-flight preparation. Furthermore, there exists a parameter CF_k which describes fixed costs for the deployment of an aircraft to solve the problem. Thus, in case of sufficiently high costs, the number of required aircraft can be reduced until the necessary minimum. The binary decision variable x_{ijk} decides whether air taxi k connects two flights i and j via arc (ij) .

Each vehicle k is equipped with an electric drive, which draws energy from a battery with a capacity of BC_k . This battery discharges during a vehicle rotation, and the current state of charge is measured before each flight i , expressed as b_{ik} . Each vertiport has infrastructure for charging the vehicle before flight i , with a charging amount of z_{ik} and a constant charging power of P^{charge} .

Notation

Sets:

\mathcal{N} set of flights with depot

\mathcal{C} set of flights

\mathcal{V} set of air taxi

\mathcal{A} set of arcs

Parameters:

CE_{ijk} edge cost, ground event

CN_{ik} node cost, flight event

C^{ARR} cost rate arrival delay

A_{ij}^{AM} 1 if flight j can be a successor of i ,
0 otherwise

A_{ik}^{AK} 1 if flight j can be served by vehicle k ,
0 otherwise

F_{ik} flight time of i with k

T_{ij} ground time between i and j

CF_k fix cost for using vehicle k

A_i, B_i open/close fix time window

$A_i, SIBT_i$ open/close soft time window

p^{charge} battery charging performance

BC_k battery capacity of vehicle k

M BigM, very large number

Variables:

x_{ijk} binary variable: 1 if flights i and j are served
by vehicle k in this order, and 0 otherwise

d_i^{ARR} arrival delay of flight i

s_i start time of flight

e_i end time of flight

v_k time vehicle k returned to depot

$hdarr_i$ help variable for delay

w_{ij} wait time before serving flight j

b_{ik} battery status of vehicle k before charging in i

z_{ik} battery charge of vehicle k before departure of i

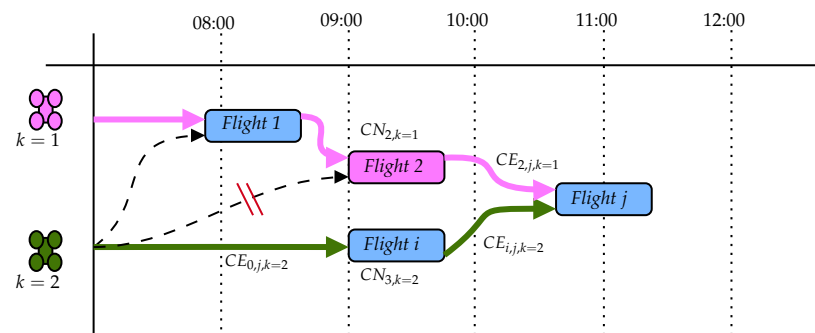


Figure 7. Schematic representation of four flights to be planned (*Flight1*, *Flight2*, *i*, *j*) as a timetable and two air taxi vehicles (magenta $k = 1$, green $k = 2$). Flights are connected with arcs (dashed: feasible connections, solid colored arrows: selected connection) which form a vehicle rotation and also consider turnaround and repositioning internally. CN represents flight operation costs and CE represents all costs associated with the linkage of two flights to an air taxi. *Flight2* cannot be serviced by air taxi $k = 2$ due to a capacity constraint.

$$\begin{aligned}
 & \min \sum_{k \in \mathcal{V}} \sum_{(ij) \in \mathcal{A}, i \geq 1} (CN_{ik} + CE_{ijk})x_{ijk} + \sum_{i \in \mathcal{C}} d_i^{ARR} C^{ARR} + \sum_{(0j) \in \mathcal{A}, j \geq 1} x_{0jk} CF_k \quad (18) \\
 \text{s.t.} \quad & \sum_{k \in \mathcal{V}} \sum_{i \in \mathcal{N}, A_{ij}^{AM} = 1} x_{ijk} = 1 \quad \forall j \in \mathcal{C} \quad (19) \\
 & \sum_{(ij) \in \mathcal{A}} x_{ijk} = 0 \quad \forall k \in \mathcal{V}, \forall i \in \mathcal{C}, A_{ik}^{AK} = 0 \quad (20) \\
 & \sum_{i \in \mathcal{N}, A_{iu}^{AM} = 1} x_{iuk} - \sum_{j \in \mathcal{N}, A_{uj}^{AM} = 1} x_{ujk} = 0 \quad \forall u \in \mathcal{C}, \forall k \in \mathcal{V} \quad (21) \\
 & \sum_{j \in \mathcal{N}, a_{0j}^{AM} = 1} x_{0jk} \leq 1 \quad \forall k \in \mathcal{V} \quad (22) \\
 & A_i \leq s_i \leq B_i \quad \forall i \in \mathcal{N} \quad (23) \\
 & A_i \leq e_i \leq B_i \quad \forall i \in \mathcal{N} \quad (24) \\
 & e_i = s_i + F_{ik} + z_{ik} \quad \forall i \in \mathcal{N}, i \geq 1, \forall k \in \mathcal{V} \quad (25) \\
 & e_i + hdarr_i - d_i^{ARR} = SIBT_i \quad \forall i \in \mathcal{C} \quad (26) \\
 & e_j - e_i + (1 - x_{ijk})M \geq F_{jk} + T_{ij} + w_{ij} + z_{jk} / P^{charge} \quad \forall (ij) \in \mathcal{A}, i, j \geq 1, \forall k \in \mathcal{V} \quad (27) \\
 & e_j - v_k + (1 - x_{0jk})M \geq F_{jk} + T_{0j} + w_{0j} + z_{0k} / P^{charge} \quad \forall j \in \mathcal{N}, a_{0j}^{AM} \geq 1, \forall k \in \mathcal{V} \quad (28) \\
 & b_{0k} = BC_k \quad \forall k \in \mathcal{V} \quad (29) \\
 & b_{jk} \leq b_{ik} + z_{ik} - CN_{ik} - CE_{ijk} + (1 - x_{ijk})M \quad \forall (ij) \in \mathcal{A} \forall k \in \mathcal{V} \quad (30) \\
 & b_{jk} \geq b_{ik} + z_{ik} - CN_{ik} - CE_{ijk} - (1 - x_{ijk})M \quad \forall (ij) \in \mathcal{A} \forall k \in \mathcal{V} \quad (31) \\
 & b_{ik} + z_{ik} \leq BC_k \quad \forall i \in \mathcal{C}, \forall k \in \mathcal{V} \quad (32) \\
 & b_{ik}, z_{ik} \geq 0 \quad \forall i \in \mathcal{C}, \forall k \in \mathcal{V} \quad (33) \\
 & x_{ijk} \in \{0, 1\} \quad \forall i, j \in \mathcal{N}, \forall k \in \mathcal{V} \quad (34)
 \end{aligned}$$

The objective Function (18) minimizes the total cost of ground and flight operations, the costs of arrival delay, and fix costs for each used air taxi (by leaving the depot). Direct operating costs related to the dummy depot are excluded.

Equation (19) guarantees that each flight is served once. The adjacency matrix A_{ik}^{AK} encodes the range, capacity, and other restrictions of the air taxis used, as well as any other relevant constraints for a specified flight. Herewith, Equation (20) avoids all flight-vehicle assignments that are undesired by the user-defined configuration. This formulation can also be used to link planned maintenance events to a specific air taxi.

By Equation (21), the flow conditions and in Equation (22) the maximum number of available air taxi is ensured. The Equations (23)–(25) provide the time restrictions of the flights, where the start and end of a flight must be within its fixed time window. Equation (25) takes care of this for calculating the arrival time of the flight at the destination.

Equation (26) measures the delay duration d_i^{ARR} per STW. This value is incorporated into the objective function along with the cost factor C^{ARR} . The Equations (27) and (28) ensure the correct computation of start and wait times and include flight, turnaround, repositioning, waiting and battery charging time. Equations (29)–(33) are essential for both the battery state of charge and the charging process at each individual station. Equation (29) ensures that each air taxi starts with its battery capacity, and Equations (30) and (31) calculate the exact battery states. The battery capacity constraints in Equation (32) ensure that battery charging must not exceed the battery capacity and Equation (33) expresses that the current battery states must be positive. Finally, the statement in (34) restricts x_{ijk} to binary conditions.

The objective Function (18) weighs various costs together. The costs CN_{ik} and CE_{ijk} represent flight operational costs, representing the consumption of electric energy in kWh of each air taxi k in the simplest case. The delay cost rate C^{ARR} occurs only if a flight is delayed and is independent of operational costs. However, the value of the fixed costs CF_k

per air taxi k determines the number of air taxis used, and in extreme cases, with very high fixed costs CF_k , only one air taxi will be used for all flights, resulting in massive delays. Since weighing these fixed costs is difficult without knowledge of investment costs for the network, we omit the third part of the objective Function (18) in subsequent discussions and instead calculate, for each scenario, the average delay per flight for a given number of available air taxis $k \in \mathcal{V}$, which we evaluate under the criterion of Pareto-optimality.

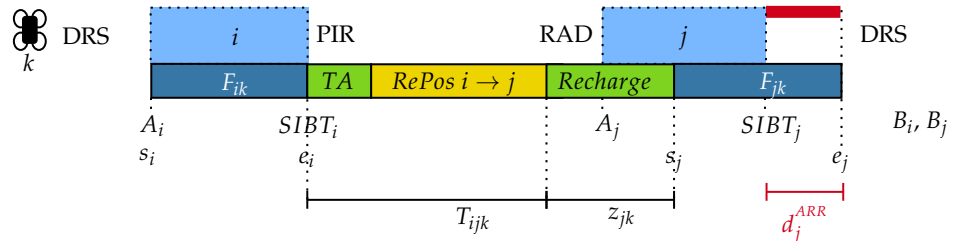


Figure 8. Two flights, i and j , are assigned to air taxi k . The light blue box represents the scheduled times based on the desired departure times, while the dark blue box represents the actual times. F_{ik} and F_{jk} describe the flight time, and T_{ijk} aggregates the necessary duration for a turnaround time between the vertiports ‘DRS’ and ‘PIR’ and the duration for repositioning between ‘PIR’ and ‘RAD’ (yellow), which is the departure location for flight j . Repositioning requires recharging of the battery (green), which means that flight j lands in ‘DRS’ with an arrival delay of d_j^{ARR} compared to the scheduled landing time $SIBT_j$ if flight j (STW).

4.2. Heuristic Solver

Large optimization problems are computationally complex and challenging to solve using exact algorithms. Heuristics are useful when dealing with problems that involve a large number of variables or constraints. Although these methods do not guarantee an optimal solution, they can often provide solutions that are close to optimal in a much shorter amount of time. For the best fit in aircraft count, the criterion of global optimality in delay and operational cost is not necessarily required to be met due to uncertainties in the model input. To tackle the problem, we implement the mathematical model described in Section 4.1 in the Java-based Optaplaner v8.36.0 framework [90], which employs a combination of construction heuristics and local optimization approaches. The tool iteratively refines candidate solutions S until a satisfactory solution is found or a stopping criterion is reached. Starting from the current solution, the tool can be configured to allow a candidate solution to bypass local optima by accepting temporarily worse solution scores.

Our decision to opt for OptaPlanner arises from its adaptability to flight schedules and other problems, its customizable evaluation function, its open-source nature, and its extensive customization capabilities for improvement strategies. Since determining the best optimization approach is beyond the scope (see Section 7.2), we are using default settings (Construction heuristic First, Fit, Metaheuristic Tabu Search). Through testing on flight scheduling instances, these settings improved solutions by less than 1% in approximately one hour. This indicates that this approach remains a practical choice for real-world issues without necessitating extensive optimization efforts on the solver approach itself. The solution time varies with problem size, and solution quality depends on complexity, particularly in generating feasible solutions via neighborhood search.

Depending on the departure and destination of flights in a solution S , repositionings and, if necessary, rechargings are inserted. The evaluation of the solution is implemented using an EasyScoreCalculator, where the HardScore HS_{c_S} of the solution S ensures compliance with the adjacency A_{ik}^{AK} of flights to air taxis and tries to avoid delays above 30 min (see pseudocode in Algorithm 1, lines 8 and 28). The SoftScore SS_{c_S} evaluates cost according to Equation (18) with CN_{ik} , CE_{ijk} and delay from d_i^{ARR} (lines 26 and 34). Two differences occur comparing the MILP from Section 4.1 and Algorithm 1: In the MILP formulation, the turnaround time T_{ijk} is independent of the charging duration. However, this time could be used for charging, mathematically formulated by an additional

BigM formulation, albeit at the expense of increasing its complexity. This is performed in Algorithm 1 by Line 19, while the battery's capacity limit is not exceeded. Further, ground idle time until the next scheduled flight can be utilized for recharging (lines 31–32).

Algorithm 1 Algorithm to calculate the score of a given AAM flight schedule solution.

Require: A solution S as list of air taxis $k \in \mathcal{V}$ and their assigned flights $i \in C$.

```

1:  $HSc \leftarrow 0, SSc \leftarrow 0$ 
2: for each air taxi  $k$  in  $\mathcal{V}$  do
3:    $Flightset_k \leftarrow$  list of flights assigned to  $k$ 
4:   if  $|Flightset_k| > 0$  then
5:      $preFl \leftarrow$  null,  $b_k \leftarrow$  battery capacity  $BC_k$  of  $k$ 
6:     for each  $curFl$  in  $Flightset_k$  do
7:       if  $k$  is not qualified to fly  $curFl$  then
8:          $HSc \leftarrow HSc - 1$ 
9:       end if
10:      if  $preFl =$  null then
11:         $preFl \leftarrow curFl$ 
12:         $preFl.actualDepTime \leftarrow curFl.scheduledDepTime$ 
13:         $preFl.actualArrTime \leftarrow preFl.actualDepTime + F_{preFl,k}$ 
14:         $b_k \leftarrow b_k - CN_{preFl,k}$  battery charging state
15:      else
16:         $T_{preFl,curFl,k} \leftarrow$  turnaround + repositioning time between  $preFl$  and  $curFl$  for  $k$ 
17:         $preFl.actualArrTime \leftarrow preFl.actualArrTime + T_{preFl,curFl,k}$ 
18:         $c \leftarrow CE_{preFl,curFl,k} + CN_{curFl,k}$  (energy consumption)
19:         $z_k \leftarrow \max(\text{charge during turnaround}, c)$ ,  $b_k + z_k \leq BC_k$ 
20:         $b_k \leftarrow b_k + z_k - c$ 
21:         $t_k^{charge} \leftarrow$  charging time required to recharge  $z$  units of battery
22:         $curFl.actualDepTime \leftarrow \max(curFl.actualDepTime + t_k^{charge}, curFl.scheduledDepTime)$ 
23:         $curFl.actualArrTime \leftarrow curFl.actualDepTime + F_{curFl,k}$ 
24:         $d_{curFl}^{ARR} \leftarrow curFl.actualArrTime - curFl.scheduledArrTime$  (delay)
25:        if  $d_{curFl}^{ARR} > 0$  then
26:           $SSc \leftarrow SSc - (d_{curFl}^{ARR})$  (delay cost)
27:          if  $d_{curFl}^{ARR} > 30$  min then
28:             $HSc \leftarrow HSc - 1$ 
29:          end if
30:        else
31:           $z_k = \min(-d_{curFl}^{ARR} \cdot P, BC_k - b_k)$ 
32:           $b_k \leftarrow b_k + z_k$  (recharge during idle)
33:        end if
34:         $SSc \leftarrow SSc - c$  (energy consumption)
35:         $preFl \leftarrow$  flight with the same parameters as  $curFl$ 
36:      end if
37:    end for
38:  end if
39: end for
40: return  $(HSc, SSc)$ 

```

5. Model Parameters for Flight Performance

5.1. Power Requirements

The computation of energy consumption for a flight entails determining the necessary power for each air taxi category and flight segment s . This is accomplished by employing the equations and assumptions for segment durations t_s outlined in Section 3.3. The resultant power requirements under MTOM conditions are presented in Table 7.

Table 7. Derived power requirements [kW] per air taxi category and flight segment according to Section 3.3.

Segment <i>s</i>	Vectored Thrust	Lift and Cruise	Multicopter
Hovertaxi	725.07	385.82	54.17
Vertical take-off	806.23	441.67	88.38
Transition	1647.64	1025.46	-
Cruise	121.40	68.99	88.29
Vertical landing	651.07	337.03	33.20
Groundtaxi	12.14	6.90	8.83

5.2. Energy Consumption

By incorporating the time durations t_s outlined in Table 5 and the required power from Table 7 into Equation (13), we ascertain the required energy for each flight segment s , consolidated in Table A2. Here, the energy demands for vertical take-off and landing, as well as for transition, are summarized depending on different assumed durations for the vertical segments. For *Multicopter* air taxi, the energy demands solely encompass vertical segments, as they do not undergo a transition phase. The cruise phase is addressed separately in Table A3 due to its dependence on distance and time factors specific to flights and particular routes.

Table A3 provides the energy consumption for the cruise phase per air taxi category, depending on the destination. In this context, the cruise distance denotes the travel distance covered while the air taxi operates at its cruise speed (derived by subtracting the acceleration and deceleration distances from the values in Table 6). Additionally, the total horizontal duration also accounts for the duration of acceleration and deceleration at cruise altitude (as presented in Table 6). This cumulative duration contributes to the overall energy consumption, calculated by multiplying the total horizontal duration by the corresponding power requirement obtained from Table 7.

Table 8 summarizes the total energy consumption and time duration for the whole flight mission and each air taxi category according to Figure 2, assuming a duration of 30 s for each take-off and landing phase, cf. Table A2. At this point, the energy consumption has to be compared to the assumed usable energy values per air taxi category shown in Table 4. Notably, the *Multicopter* is limited to short distances, such as Neustadt/S., since Chemnitz and Leipzig exceed its usable energy capacity. Conversely, the other air taxi categories face no challenges and can be assigned to all specified routes within the use case network from an energy perspective.

Table 8. Total energy consumption and duration for whole flight mission per air taxi category depending on the destinations.

Destination	Vectored Thrust		Lift and Cruise		Multicopter	
	Total Energy Demand [kWh]	Total Duration [min]	Total Energy Demand [kWh]	Total Duration [min]	Total Energy Demand [kWh]	Total Duration [min]
Kreischa	44.8	6.7	27.9	8.5	14.7	10.9
Moritzburg	45.1	6.9	28.2	8.8	15.4	11.4
Wilsdruff	45.7	7.2	28.8	9.3	16.7	12.3
Ottendorf-Okr.	46.9	7.8	30.1	10.4	19.4	14.1
Pirna	47.3	8.0	30.5	10.8	20.3	14.8
Dippoldisw.	47.6	8.1	30.8	11.0	20.8	15.1
Meißen	49.6	9.1	32.9	12.8	25.3	18.2
Glashütte	49.7	9.1	32.9	12.9	25.4	18.2
Altenberg	54.1	11.3	37.4	16.8	35.0	24.8
Neustadt/S.	54.9	11.7	38.2	17.5	36.8	25.9
Chemnitz	68.3	18.3	51.9	29.4	66.0	45.8
Leipzig	86.0	27.1	70.0	45.2	104.6	72.1

5.3. Air Taxi Payload over Range

Due to the divergence between the achievable energy and the corresponding energy demand based on the destination, this section outlines the maximum range for all air taxi categories. As detailed in Table A2, the energy requirements for all flight segments (excluding the cruise phase) are elucidated under MTOM conditions. With a vertical duration of 30 s, the total energy consumption per air taxi category can be concisely summarized as:

$$6.04 \text{ kW h} + 15.87 \text{ kW h} + 14.59 \text{ kW h} + 0.10 \text{ kW h} = 36.6 \text{ kW h for Vektored Thrust,} \quad (35)$$

$$3.22 \text{ kW h} + 9.38 \text{ kW h} + 8.51 \text{ kW h} + 0.06 \text{ kW h} = 21.16 \text{ kW h for Lift and Cruise, and} \quad (36)$$

$$0.45 \text{ kW h} + 0.74 \text{ kW h} + 0.28 \text{ kW h} + 0.07 \text{ kW h} = 1.54 \text{ kW h for Multicopter.} \quad (37)$$

By subtracting these values from the corresponding usable energies (based on a specific energy density of 200 W h kg^{-1}), the usable amounts of energy for cruise flight per air taxi category are obtained:

$$110.96 \text{ kW h} - 36.6 \text{ kW h} = 74.36 \text{ kW h for Vektored Thrust,} \quad (38)$$

$$80.56 \text{ kW h} - 21.16 \text{ kW h} = 59.4 \text{ kW h for Lift and Cruise, and} \quad (39)$$

$$45.6 \text{ kW h} - 1.54 \text{ kW h} = 44.06 \text{ kW h for Multicopter.} \quad (40)$$

Multiplying these values with the estimated power requirements (refer to Table 7) per air taxi category for the cruise phase enables the calculation of the time required to consume this energy, corresponding to the total duration of the cruise flight. These time durations need to be adjusted by the durations of acceleration and deceleration (refer to Table 6) to estimate the time during which the air taxis maintain a constant speed:

$$\frac{74.36 \text{ kW h}}{121.40 \text{ kW}} \cdot 3600 \text{ s h}^{-1} - 33 \text{ s} - 120 \text{ s} = 2052 \text{ s for Vektored Thrust,} \quad (41)$$

$$\frac{59.4 \text{ kW h}}{68.99 \text{ kW}} \cdot 3600 \text{ s h}^{-1} - 26 \text{ s} - 80 \text{ s} = 2994 \text{ s for Lift and Cruise, and} \quad (42)$$

$$\frac{44.06 \text{ kW h}}{88.29 \text{ kW}} \cdot 3600 \text{ s h}^{-1} - 22 \text{ s} - 60 \text{ s} = 1715 \text{ s for Multicopter.} \quad (43)$$

Multiplying these times with the corresponding cruise speeds and considering the distances for acceleration and deceleration delivers the maximum range of each air taxi category under MTOM conditions (see Table 6):

$$2052 \text{ s} \cdot 72 \text{ m s}^{-1} + 1177 \text{ m} + 4320 \text{ m} = 153 \text{ km for Vektored Thrust,} \quad (44)$$

$$2994 \text{ s} \cdot 40 \text{ m s}^{-1} + 519 \text{ m} + 1600 \text{ m} = 122 \text{ km for Lift and Cruise, and} \quad (45)$$

$$1715 \text{ s} \cdot 24 \text{ m s}^{-1} + 262 \text{ m} + 720 \text{ m} = 42 \text{ km for Multicopter.} \quad (46)$$

The mass of the air taxi affects the power requirements for the different flight segments. In principle, the power requirements decrease the lower the air taxi mass which, in turn, depends on the load factor (number of passengers carried). This also results in higher maximum ranges, which is shown by the solid lines in Figure 9. Additionally, the entire calculation is also conducted for a specific energy density value of 250 W h kg^{-1} . In this case, the maximum range increases as shown by the dashed lines in Figure 9. Generally, the diagram indicates possible flight distances depending on the used payload.

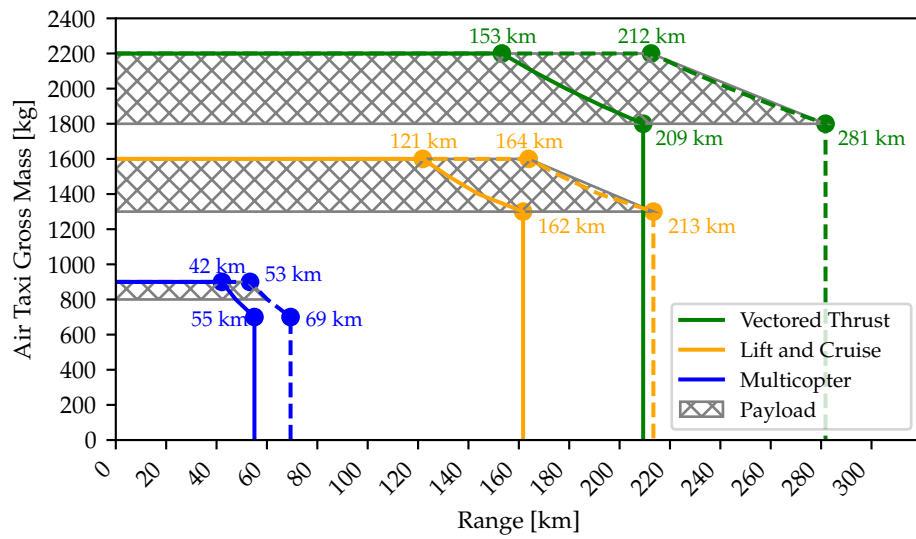


Figure 9. Payload-range diagram per air taxi category for an energy density of 200 Wh kg^{-1} (solid lines) and an increased energy density of 250 Wh kg^{-1} (dashed).

Air Taxi Turnaround

The turnaround is necessary to prepare the air taxi for the next flight. According to Section 2.2, aircraft handling processes for air taxi operations are reduced to a passenger-centric path, recharging, and minor MRO tasks.

In case there is no recharging required (e.g., the battery capacity is still sufficient for the subsequent flight), the turnaround duration is determined by the duration of de-boarding and boarding. Hence, this is dependent on the passenger capacity and the resulting time each passenger needs to disembark and embark on the air taxi. In [42], this duration is assumed by one minute per passenger, which leads to turnaround durations of 13 min for *Vectored Thrust*, 11 min for *Lift and Cruise*, and 7 min for *Multicopter*. The complete durations are visualized per air taxi category in Figure 10. The chosen colors reflect the corresponding air taxi categories as in Figure 9.

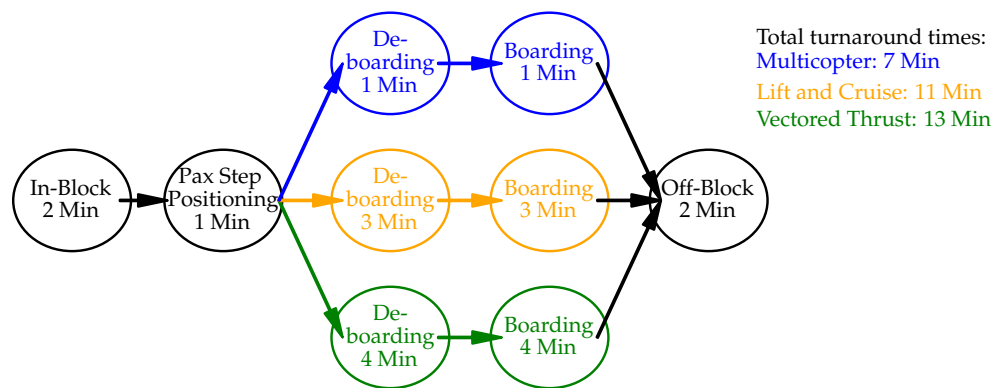


Figure 10. Turnaround time T_{ijk} per air taxi category, excluding flight-dependent battery charging times.

The recharging can be the most time-consuming phase during turnaround and is on the critical path. In [42], different applications for restoring the battery capacity are examined (plug-in charging, battery swapping, and underbody charging technology). Here, the used approach for estimating the charging time t^{charge} is approximated by dividing the

amount of energy to be recharged E [kW h] by the charging power P_t^{charge} provided by the infrastructure (Equation (47)):

$$t^{charge} = \frac{E}{P_t^{charge}}. \quad (47)$$

6. Results

This section evaluates the network performance and determines the necessary number of air taxis (Section 6.1) to meet the requirements of the use case presented in Section 3.1. Additionally, it explores the impact of specific parameters in Section 6.2 (such as turnaround and charging time, demand) on the optimal fleet size and the resulting delay.

6.1. Fleet Sizing Based on Flight Scheduling

6.1.1. Average Delay in the Standard Demand Scenario

For the case study with the demand outlined in Section 3.1, we identified a total of 388 flights by aggregating passengers with the same departure time, destination, and considering available seat capacity. The problem is solved with the approach described in Section 4.2. In the absence of a distinct stopping criterion for the local search heuristic, we limited the computation time to a maximum of 6 h per individual model run. Additionally, the solver is authorized to finish if the objective function value was not improved within a 2 h timeframe. Our computational infrastructure is powered by a 12-core Intel Xeon Gold 6136 CPU, resulting in an approximate solution generation and evaluation velocity of 90,200 possible solutions per second. We use an acceptance threshold of 4 min delay per flight, aligning with common metrics in airport capacity design [91].

The schedule depicted in Figure 11 provides a snapshot of the complete schedule with 32 aircraft. This solution is selected based on the best balance between the number of required air taxis and the resultant average delay. In instances with fewer air taxis, the delay situation worsens (as indicated by red bars in Figure 11). Conversely, a higher number of aircraft leads to a consistent improvement in the situation. Typically, flight delays accumulate in the afternoon due to increased demand compared to the morning/noon, along with cascading effects in downstream schedules. In this context, a delay is defined as a variance from the scheduled times compared to the intended arrival time based on traffic demand. It should be perceived as a deviation from the ideal flight schedule rather than passenger disruptions during flight operations. Additionally, the schedule reveals frequent battery recharges (green bars), interspersed with aircraft repositionings (yellow bars). In general, a total energy consumption of 17,200 kW h for all flights is expected, which corresponds to approximately 44 kW h per flight.

Figure 12 shows the correlation between the average flight delay and the number of available vehicles, resulting in a Pareto frontier. Between 20 and 30 air taxis, there is a significant drop in the average delay. The findings reveal that by utilizing a fleet of 32 air taxis, the requirement of an acceptable delay threshold is met, resulting in a total delay of 980 min and an average delay of 2.5 min per flight. To maintain an average delay of no more than 1 min per flight, a minimum of 35 air taxis is necessary, while a negligible delay averaging 0.1 min per flight necessitates at least 46 air taxis. These findings underscore that tolerating a delay can lead to an almost 25% reduction in the number of air taxis compared to a delay-free scenario. The impact of this slight delay on the flight schedule is minimal due to its minor ratio compared to the flight duration. Consequently, aircraft utilization and network productivity are higher compared to the no-delay solution (6.9 flight hours per day and air taxi compared to 4.9 flight hours at no delay with 46 air taxis). These results assume an uninterrupted flight operation and thus represent the lower limit of required air taxis. An additional buffer should be planned for disruptions and maintenance.

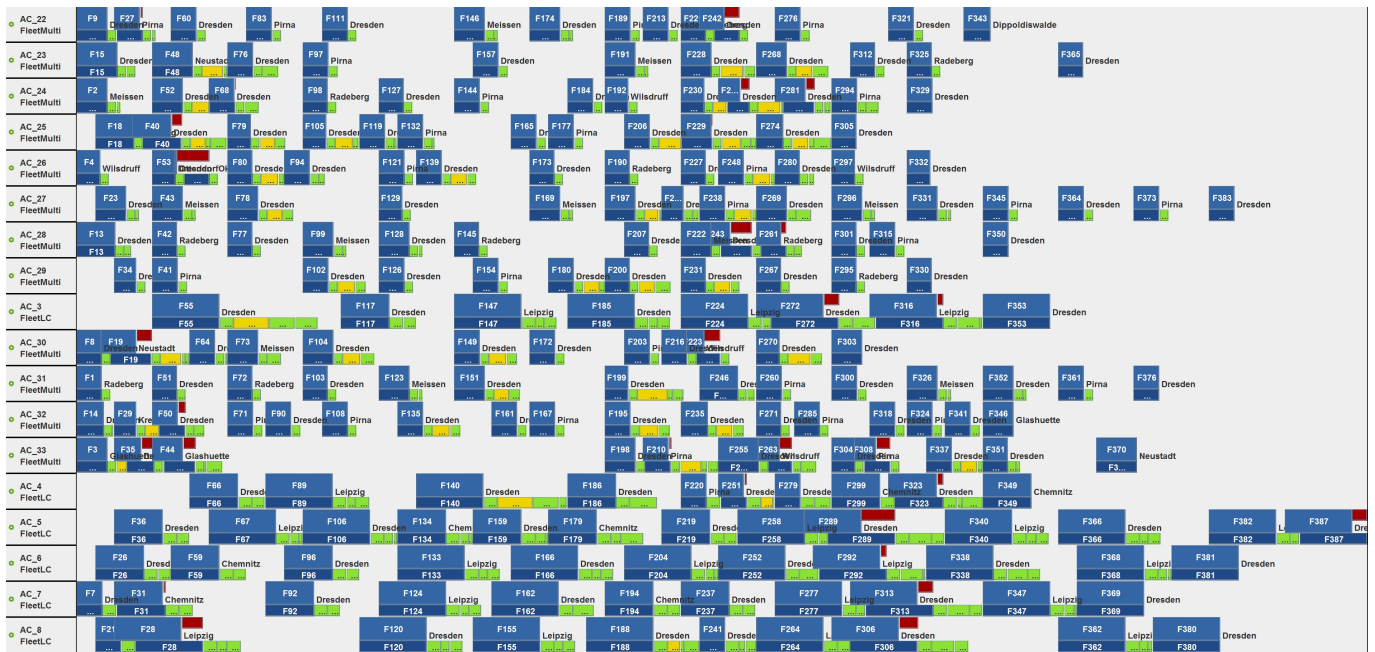


Figure 11. A total of 18 air taxis out of a schedule with 32 vehicles: some minor delays (red) at the peaks in traffic demand, and frequent battery recharging (green bars), as well as infrequent repositionings (yellow bars) are observed.

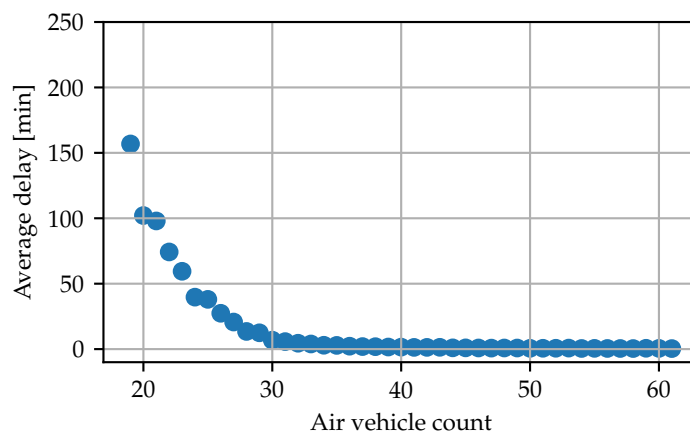


Figure 12. Standard demand scenario: average delay per flight as a function of the number of air taxis serving 388 flights per day.

For evaluating termination criteria and computation time, Figure 13 illustrates the convergence of the objective value as a function of time for the case of now 37 air taxis. This case represents the most computationally intensive calculation among the scenarios in Figure 12. Here, the best objective value was finally found after 3.5h, approximately 2.5h before the time limit. From the curve in Figure 13, it can be observed that the solver already found a good solution after approximately 50 min. This corresponds to less than 14% of the available computation time and 24% of the actually needed time. From this point on, the average delay only marginally changes from the value of 247 min total delay to 215 min in the final solution (0.6 min per flight). This implies that further extensive solution search is improbable to significantly improve the delay situation. Thus, the local optimality of the solution appears to be sufficient, especially when considering the absolute differences in solution quality, particularly when uncertainties from the scenario setting are considered. All other scenarios from Figure 12 required less computation time to converge. On average across all scenarios, the required computation time, evaluated based on the

last improvement in the found score, is 1.65 h, with the observation that a few air taxis contribute to the fastest convergence of the score due to less complexity.

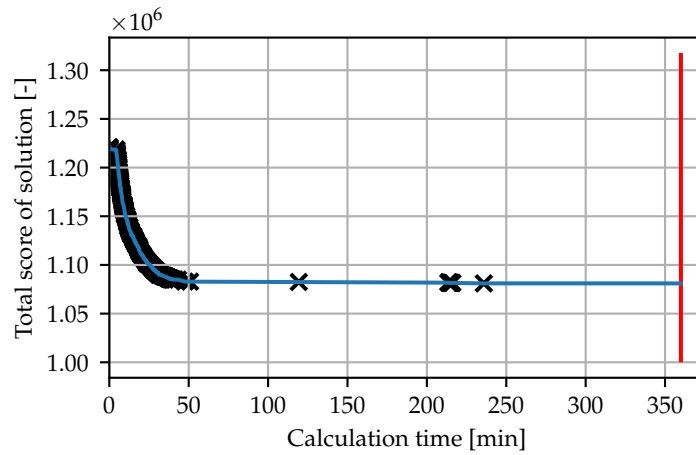


Figure 13. Calculation time for flight schedule with 37 air taxis in the standard demand scenario, with black markers indicating improvements to the current best solution score (delay and operations cost) and a red line representing the user-defined time limit; a total of 0.6 min of delay per flight were measured.

6.1.2. Best Solution Characteristics (32 Air Taxi)

Based on the analysis in Figure 12, we find that the network runs well with an average delay of under 4 min per flight using only 32 air taxis. This solution is selected as the *best* one, meeting the delay target while minimizing the number of air taxis required. The histogram in Figure 14 displays delay frequency based on this solution. Out of 388 flights, 79 depart after their preferred time, with around 24% of those having delays of less than 5 min—a level acceptable to customers. Conversely, about 6% of flights encounter delays of at least 15 min, which might reduce network appeal (≥ 30 min: 0.8%). While an outlier reached 107 min of delay, very high delays are rare. Introducing more air taxis decreases high delays but increases the number of shorter ones. Delays exceeding 30 min can be completely avoided with a minimum of 34 air taxis (longest delay: 28 min).

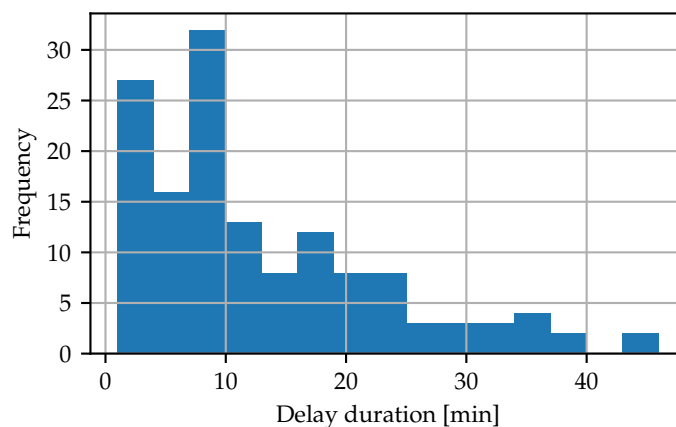


Figure 14. Distribution of flight delay in the *best* solution with 32 air taxis. One flight with 107 min delay is excluded from this figure.

In scenarios where flight schedules involve an air taxi count definitively avoid any delay (≥ 60) and allow increased flexibility in flight scheduling, an optimal fleet mix has been identified for this network. This fleet is comprised 10% *Vectored Thrust* aircraft, 50% *Lift and Cruise* aircraft, and the remaining 40% are *Multicopter* aircraft. This allocation takes

into account factors such as demand, available seating capacity, and flight performance, with a primary focus on cruising speed and disregarding initial investment costs. Notably, flight performance considerations prioritize available seating capacity over cruising speed. This emphasis is evident in the average flight duration per aircraft, as detailed in Table 9. The fleet distribution exhibits significant diversity, with *Multicopters* predominantly serving shorter flights, resulting in lower daily utilization rates (productive flight time proportion). *Multicopters* excel in frequent short trips, aligning well with urban mobility requirements. On the other hand, *Lift and Cruise* vehicles demonstrate efficiency in long-distance travel, aligning with the regional transportation focus of our network. These conclusions are specific to the network under consideration and may vary for different distances and demand patterns.

Given a charging power of $P^{charge} = 150$ kW, a total of 746 recharge events were observed across the entire flight schedule, with an average duration of 10.2 min. Recharging events can be classified into three categories: (a) recharging during the turnaround period, (b) standard recharging after the turnaround to meet energy requirements before the flight, and (c) recharging during ground idle phases until the next scheduled flight. With these distinctions, 407 merged charging sessions were identified, demonstrating an average duration of 18 min. As the cumulative charging duration nearly matches the actual flight durations, battery recharging plays a significant role in the daily operations of air taxis. Thus, enhancing the charging power P^{charge} beyond the assumed 150 kW would substantially enhance productivity (cf. Section 6.2.2). Furthermore, a total of 59 repositioning flights, serving as empty flights between destinations and departures, were found in the schedule, with an average duration of 8 min (mostly observed in the Dresden–Pirna route). In this case, repositioning flights account for approximately 13% of all executed flights. These arise from the network structure and distribution of the demand together with prioritizing a less aircraft count, substantially limit the productivity of air taxis. However, since repositioning also contributes to the overall charging duration, reductions are desired. For instance, centralizing operations within the network through traffic bundling or increasing the availability of air taxis can effectively reduce the necessity for repositioning (see Section 6.1.3). Finally, based on this network, demand and accepting 4 min delay per flight, the 32 air taxi transport in total 37,765 passenger kilometers (pkm) of demand (1180 pkm per air taxi).

Table 9. Utilization of each fleet in the standard demand scenario, considering a total of 32 air taxis serving the network from Section 3.1.

	<i>Vectored Thrust</i>	<i>Lift and Cruise</i>	<i>Multicopter</i>
Use Share	10%	50%	40%
Avg. flight count per vehicle	9.3	10.6	14.5
Avg. vehicle utilization [h day ⁻¹]	5.5	8.4	5.3
Avg. recharge count per vehicle	8.6	10.5	16.3
Avg. recharge event (merged) [min]	35.6	26.5	10.2
Avg. duration of recharge [h vehicle ⁻¹]	5.1	4.6	2.8
Avg. reposition count per vehicle	2	1.5	3.5
Avg. duration of reposition [h vehicle ⁻¹]	0.43	0.28	0.4
Avg. distance per flight [km]	90	84	19
Avg. consumption per flight [kW h]	84	64	21
Avg. consumption per vehicle/day [kW h]	811	681	302

6.1.3. Effect of Repositioning Flights on Efficiency

In general, repositioning flights are the effect of the limited number of available air taxis and have a notable impact on flight efficiency. These flights not only consume additional time and aircraft resources, but also result in extra energy and maintenance costs, potentially disrupting scheduling and introducing delays during the day of operations. In the case of 32 air taxis and 59 repositioning flights, the energy consumption of 19,100 kW h

represents approximately 110% of the required energy for operating only flights with scheduled payload.

The relationship between repositioning flights and the number of air taxis is depicted in Figure 15a. As the number of air taxis increases, both the number of repositioning flights (in green) and their total flight time decrease (in blue), with the average duration per repositioning flight dropping from approximately 9 min to 8 min. This has positive implications for operational costs and provides a compelling argument for deploying a higher number of aircraft. Increasing from 32 to 40 air taxis, for example, could save the energy equivalent of 800 kWh. Despite the substantial quantity of air taxis, a significant number of repositioning flights persist, primarily due to the trade-off involving delay costs associated with peak periods in the flight schedule.

Additionally, Figure 15b illustrates the trend in the number and total duration of charging events concerning the number of air taxis. The number of charging events (shown in green) steadily decreases as the number of available aircraft increases, resulting in fewer required repositioning flights. However, this effect is not observed in the total charging time (indicated in blue). Instead, the total charging duration increases between 32 (highest productivity by our definition) and 44 air taxis, and then slightly decreases afterward. On average, the total charging time is 7484 min with a standard deviation of 126 min, which is relatively low. Additionally, as the number of air taxis increases, there is a consistent rise in the average charging time per charging event (without a separate illustration). This demonstrates a tactical redistribution of the charging times and places. Importantly, the seemingly longer charging duration does not negatively impact the objective function, and consequently, it does not adversely affect productivity.

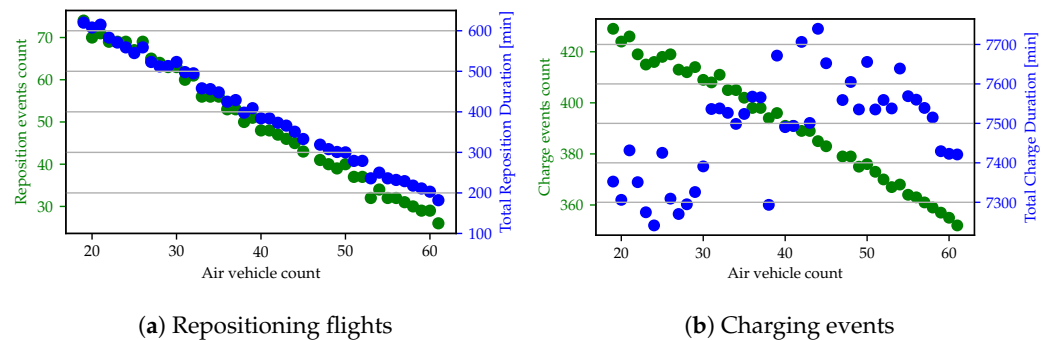


Figure 15. Number and duration of repositioning flights and recharging events as a function of available aircraft to serve the network from Section 3.1.

6.2. Parameter Study; Standard Demand Scenario, 32 Air Taxis

The optimization model involves several additional parameters, each with an impact on network performance. This section evaluates these parameters in terms of overall network efficiency and effectiveness, with a primary focus on ground time—specifically, the duration of turnaround and charging. While improving flight speed and/or battery capacity is a viable option, a significant increase in both factors is unlikely due to physical constraints. This limitation diminishes their influence on the required vehicles for network optimization.

6.2.1. Turnaround Time

The assumed turnaround durations T_{ijk} indicated in Figure 10 represent the ideal state during flight operations. However, increased taxi durations, additional waiting times for clearance, or uncertainties due to delayed start of the turnaround caused by insufficient resources can significantly extend this duration. As illustrated in Figure 11, the turnaround time is generally short when compared to other events like flying and repositioning. Nonetheless, it is part of the rotations that already experience delays due to tightly scheduled operations. To assess the influence of this uncertainty, the turnaround

times T_{ijk} are gradually increased during a sensitivity analysis spanning from a factor of 1.0 to 4.0.

It can be observed in Figure 16 that the average flight delay increases with higher turnaround durations T_{ijk} . Fundamentally, it becomes apparent that a slightly higher duration T_{ijk} initially has minimal impact on the average delay. This is attributed to the permissible parallel charging during the turnaround, as charging occupies the most portion of time. At a factor of approximately 1.3 for T_{ijk} , the turnaround starts to become predominant and exerts a more substantial influence on air taxi productivity.

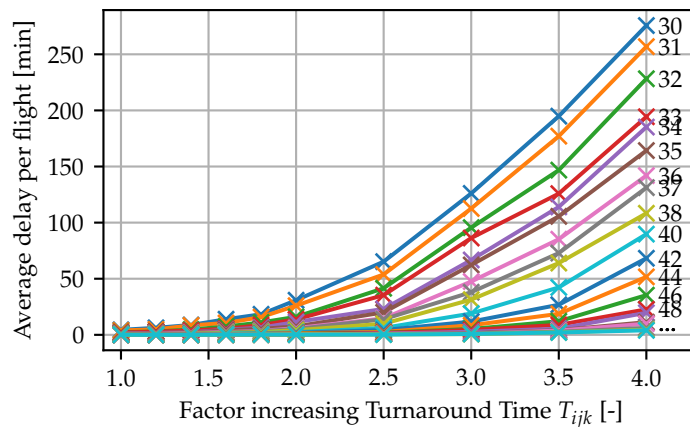


Figure 16. Averageflight delay trends with varying turnaround times T_{ijk} between factor 1.0 and 4.0 and based on the scenario parameters from Section 3.1.

An operational realistic value for the turnaround time could involve doubling the original assumption for T_{ijk} , solely due to minor operational delays in passenger processing on the day of operation. Under this scenario, assuming a consistent fleet size of 32 air taxis, the average delay increases to 16 min—a sudden quadrupling beyond the designated delay threshold. To avoid this and remain below the threshold, at least 37 air taxis are necessary for the network. With higher factors applied to T_{ijk} , the average delay significantly and rapidly increases.

6.2.2. Charging Performance

Charging accounts for 55% of the total air time in the 32 air taxi solution (flight and repositioning time). Notably, the charging duration for the *Vectored Thrust* is significantly impacted by its substantial energy consumption and is disproportionately affected by high energy consumption due to its mass. In fact, the charging time for *Vectored Thrust* amounts to 926 min, and is nearly as long as its air time of 942 min. However, the charging power of 150 kW is quite low and is already achieved with today’s car charging stations. This is likely to be far exceeded in regular air taxi operations in the future. By increasing the charging power P_t^{charge} up to 1000 kW, a reduced time required for charging and a higher air taxi utilization can be assumed. Figure 17 shows this for the gradual improvement in the charging power for the case of 32 available air taxis according to the best solution from Figure 12.

It is apparent that the total charging duration (blue) decreases with increasing P_t^{charge} . This decrease is not linear, as the solver can now use other options from the flight schedule to better utilize idle times. Interestingly, at a P_t^{charge} of 450 kW and above, charging only occurs during the turnaround phase. This can be seen from the orange line, which sums all charging events other charging events excluding during turnaround and approaches a duration of 0 at this charging power. This effect finally reduces delay, as charging is no longer the critical path in the turnaround, and the charging stations are not occupied by air taxis during idle times on the ground. This decrease in delay is also depicted by the red line in Figure 17, demonstrating a decline from approximately 1700 min total delay to roughly

a quarter, around 390 min of total delay, even when using the 400 kW charging power. Notably, increasing the charging power beyond this point does not result in a significant further delay reduction.

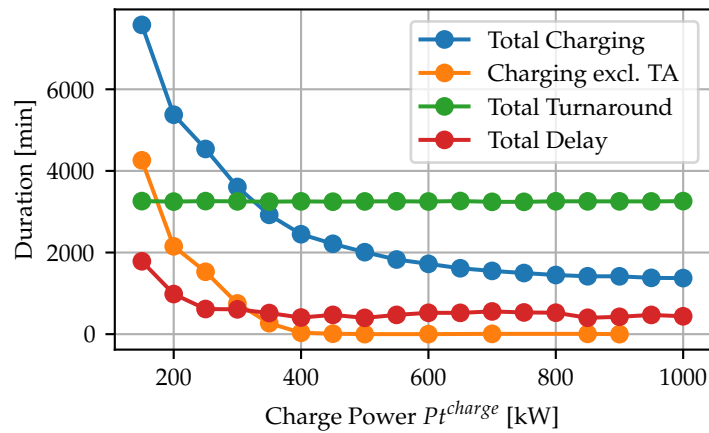


Figure 17. Total delay and charging duration while increasing the charging power P_t^{charge} , best solution with 32 air taxis.

A higher charging power naturally increases the possible air taxi productivity if a higher accepted delay level is set. With the assumptions from Section 6.1 and an average charging power of $P_t^{charge} = 450$ kW, 27 aircraft can also operate the existing flight schedule at an average delay below 4 min per flight. The corresponding aircraft utilization is then 8.5 h air time per day.

The resulting flight schedule enables an estimation of the required charging points at various locations within the network. Illustrated in Figure 18, the distribution is synchronized with the timeline presented in Figure 11, progressing from left to right. Each data point signifies a 5 min time slot, with its color denoting the number of parallel charging activities (blue: at least one air taxi charge in this slot). As an outcome of network design, charging predominantly occurs in the cities of Chemnitz, Dresden, and Leipzig. Dresden, serving as the envisaged hub for traffic flows in the network, necessitates the highest number of charging stations.

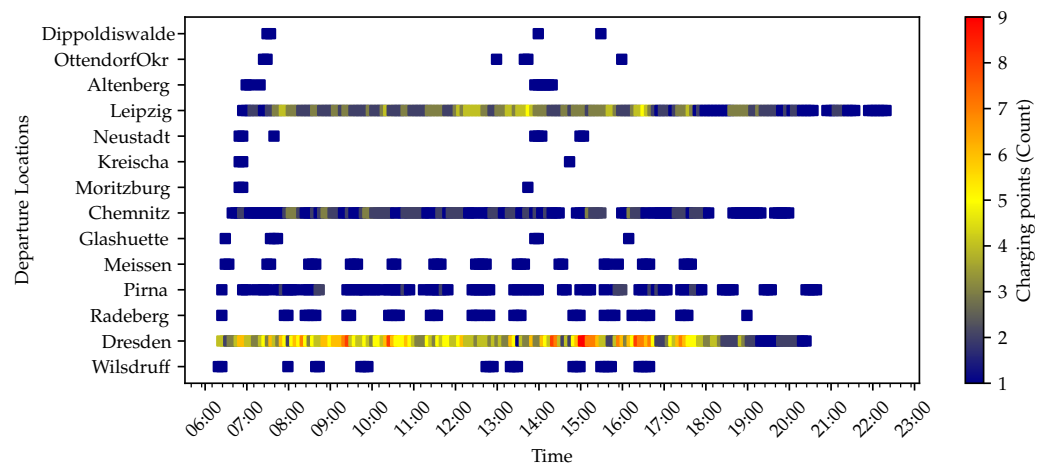


Figure 18. Required parallel charging points for air taxis at respective stations in the network is based on the assumed demand distribution throughout the day.

On average, the vertiport in Dresden requires 4.2 parallel charging points, with a maximum demand of nine concurrent charging sessions at 15:00. Chemnitz averages 1.5 (max three) charging points, while Leipzig averages 2.4 (max five). Making sure there are

enough parallel charging points in Dresden is very important to meet network needs and avoid delay. Conversely, many other locations that are infrequently serviced experience sparse charging activities. At several of these locations, such as Dippoldiswalde, the installation of charging stations may be dispensable provided that the battery capacity is sufficient for round-trip flights without intermediate charging.

6.3. Changes in Forecasted Demand

The preceding analysis assumes a standard scenario for demand, which, given the forecasting period and the novelty of the transportation mode with limited prior experience, remains uncertain. Consequently, various scenarios of altered demand are subsequently considered to contextualize the earlier results. Demand is scaled from the standard scenario and projected onto flight schedules, ranging from a 30% increase to a 30% reduction. Throughout this scaling process, the fundamental network structure of the air taxi standard network is preserved. As a result, connections with higher flight frequencies in the standard scenario are more likely to receive additional flights in the case of higher-scaled demand, while less frequented connections stand a higher chance of experiencing a reduction in flights in the case of decreased demand.

Figure 19 illustrates the effects of modified demand scenarios on average flight delay based on the number of available air taxis. The red curve corresponds to the standard scenario from Figure 12, the green curves depict a reduction in traffic demand, and the blue curves indicate an increase. The dashed line represents an approximation of the data using a Savitzky–Golay filter for visualization.

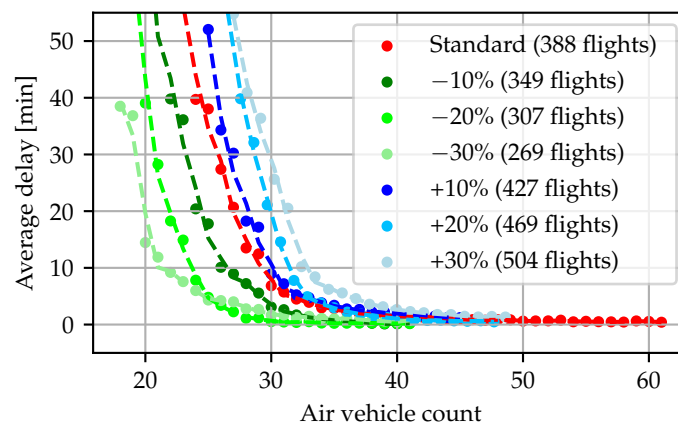


Figure 19. Impact of varying demand on average flight delay and required number of air taxis.

In Figure 19, it is shown that the average delay changes proportionally with an increase or decrease in traffic when the number of air taxis remains constant. In the case of 32 air taxis, which represent the optimal solution for the standard scenario, a 10% reduction in flights already leads to a significant 60% reduction in delays. With even lower traffic demand (−20%), the average delay decreases to only 0.4 min, representing a reduction of over 90%. To meet the previous criterion of an average delay of 4 min per flight, the number of air taxis in the system can be reduced: Assuming all other conditions remain constant, in the case of a −10% reduction in traffic, only 30 air taxis are required (−20% traffic: 27 air taxis, −30% traffic: 26 air taxis). This indicates that inferring the required number of air taxis from the number of flights cannot be accurately achieved through a linear scaling factor, even for a similar network. While this approach may yield accurate results for smaller demand scaling factors, the error in estimating the required number of air taxis increases with higher scaling factors, resulting in an underestimation of the necessary air taxis. The primary reason for this discrepancy is the frequent need for repositioning flights to meet demand, which, despite being a flight, still occupies the capacity of air taxis.

In the case of an increase in forecasted traffic, a similar trend is observed in the development of required air taxis. In this context, growth in demand results in an increased number of necessary air taxis, even when the distances between the curves are noticeably narrower (+10%: 33, +20%: 34, +30%: 37 air taxis). Consequently, the rate of increase in the vehicle count is lower than in the case of decreasing demand, primarily attributed to the solver having greater flexibility in adjusting flight schedules and avoiding the need for repositioning flights. Consequently, the error in estimating the correct number of air taxis based on traffic data using a linear factor is lower than in the case of conservative traffic forecasts.

7. Discussion

7.1. Practical and Theoretical Implications

In the preceding sections, we investigated an air taxi network's operational dynamics under various fleet-sizing scenarios for Advanced Air Mobility (AAM). We created a model to predict the number of air taxis required based on AAM demand, illustrating its application in a specific case in Saxony. This section discusses the implications of our findings, placing them in the context of prior studies and addressing our research questions.

In addition to predicting traffic demand for AAM, our primary focus lies in seamlessly integrating daily flights and a predetermined quantity of air taxis into a comprehensive flight schedule. The cornerstone of our investigation is our MILP optimization model, designed to compute a cost-minimum flight schedule and air taxi assignment. Each air taxi is categorized as one of three types: *Vectored Thrust*, *Lift and Cruise*, and *Multicopter*. For each type, we detail flight performance, energy consumption, and process duration, calculating a rotation plan for each air taxi of a given type, inclusive of repositioning flights and battery charging times.

The model further introduces the capability to incorporate a planned delay into the system. This planned delay, set at an acceptable 4 min per flight, remains imperceptible to passengers during the day of operation. Instead, it serves as a metric measuring the deviation from preferred departure times derived from initial demand data in comparison to the actual flight schedule. While moderate delays have the potential to enhance system efficiency and reduce the number of required air taxis, excessive delays deviate departure times too significantly from the ideal, eliminating crucial time buffers from the schedule. Aligning with established practices in airport capacity assessments, the considered 4 min delay per flight ensures a balanced approach to system optimization.

Given the early stage of air taxi technology and the absence of regulatory approval or operational experience, our study necessitated several key assumptions. A crucial assumption involved the development of a streamlined air taxi demand network, focusing on flights to and from Dresden—the epicenter of the network. This network is informed by previous studies [5,74], utilizing current mobility data and a daily traffic pattern derived from a survey on potential shifts to air taxis [29]. These findings are extrapolated to encompass the entire population of specific locations within the network. Notably, the assumed modal shift rates play a significant role in influencing the outcome as trips per day, with other studies highlighting their dependence on future air taxi prices.

In addition, further assumptions were introduced, potentially exerting a significant impact on the results. The assumption of uninterrupted flight operations, while aiding in modeling, may oversimplify the practical complexities of travel. Uncertainties, including specific assumptions related to aircraft performance, demand projections, and flight durations, are context-dependent and may not universally hold true for all AAM scenarios. These assumptions underscore the need for a nuanced understanding of the limitations and contextual relevance of our study's findings. In our work, we have demonstrated how a change in parameters affects the outcome for the respective network.

In the optimal solution for the defined standard of our case study with a specific demand distribution and air taxi performance parameters, we achieve an average daily utilization of approximately 6.9 flight hours per day of operation within the operational timeframe from 6 a.m. to 10 p.m. (no nighttime operations, i.e., 16 h). Events of non-availability, such as maintenance, must be factored in based on their duration. In the context of an adequately sized fleet and an accepted average delay of 4 min per flight, identified in the optimal solution, a notable portion (30%) of delay events is short-lived, lasting less than 5 min. Instances of longer delays are rare, indicating that delays within the accepted threshold minimally impact the resulting flight schedule. As the predefined threshold for tolerated delay increases, the daily utilization of air taxis rises. Simultaneously, the integration of additional air taxis into the flight plan effectively mitigates unacceptable delays.

The flight schedule inherently reflects the performance characteristics of the three categories of air taxis. *Multicopters*, despite having a comparable number of daily flights, exhibit lower average distance and total consumption due to their limited battery capacity and speed. Consequently, they are well-suited for short-distance operations within our network, covering a maximum distance of approximately 30 km. This fleet is particularly suitable for mobility in urban regions, where flight distances and charging times are correspondingly low. While *Multicopters* complete more cycles due to their shorter range, *Lift and Cruise* air taxis prove to be more efficient on longer routes and are accordingly assigned to such routes. *Vectored Thrust*, although used less frequently due to higher energy consumption, serves longer routes and could gain popularity with increasing demand due to their higher seating capacity.

The flight schedule includes unintended repositioning flights with additional operating costs depending on the network, demand distribution, and the goal of maximizing air taxi utilization. Their number decreases with a higher number of available air taxis, as more air taxis allow for idle times at individual stations, eliminating the need for virtual delay. Moreover, the schedule encompasses numerous charging events, which, with a 150 kW charging power, are nearly as long as the flight operations themselves. Increasing the charging power to around 450 kW results in shorter charging times, enhancing productivity by up to 20%, equivalent to about 1.3 flight hours per air taxi per day. This productivity increase primarily occurs during assumed turnaround times, making them a critical path. The assumption here is that charging is performed at full power as soon as the air taxi is on-site. While pre- and post-preparation tasks for charging could potentially impact productivity, they are not considered at this stage and can be adjusted by increasing the durations for ground activities, which inherently restrict charging.

Contrary to the hypothesis that uncertainty in demand estimation can be addressed solely by scaling the number of air taxis based on daily utilization and available passenger kilometers per air taxi, our findings do not confirm this approach. While effective for minor variations (up to 10%) in demand, larger deviations result in an increasing error, leading to an underestimation of the actual required number of air taxis.

7.2. Conclusions and Future Research

Our findings demonstrate the suitability of our approach in determining fleet size according to demand. Essential parameters such as loading time, flight time, etc., can be modeled and integrated into the evaluation function. Utilizing heuristics, qualitatively excellent results can be achieved within acceptable computation times. In conclusion, our results, coupled with insights from the parameter study, contribute to a comprehensive understanding of the robustness and adaptability of AAM and air taxi networks under various demand scenarios.

Given the novelty of this transportation mode, limited scientific literature focuses on AAM demand and their networks. Existing studies diverge significantly, each highlighting unique aspects, e.g., transport simulation with modeled air taxi agents [17,19,34,92]. Notably, there are no directly comparable studies known concerning demand estimation,

fleet planning, and while accepting moderate flight delays for rural areas. Furthermore, all known studies share a commonality in making specific assumptions regarding potential demand and the technical characteristics of air taxis, with the modal shift rate towards AAM being particularly uncertain [29]. Despite the divergent scopes of these case studies, certain similarities, such as the average utilization of air taxis found, suggest methodological robustness.

Moving forward, it is important to mention the need for a buffer to handle disruptions or maintenance for practical implementation as a robust solution. There is a great opportunity to enhance the simulation model by incorporating knowledge from commercial aviation flight traffic and delay statistics. Additionally, for a more comprehensive understanding, future research will explore additional demand scenarios beyond the current scaled model. Examples include scenarios with uniformly distributed and symmetrically shaped demand throughout the day or scenarios reflecting daily patterns and asymmetry. However, increased detailing is anticipated to introduce more complexity and computational challenges in solving the optimization problem. A subsequent focus on identifying suitable heuristics is expected to expedite solutions, particularly when experimenting with various scenarios. Simultaneously, highly adaptable simulation-based approaches, e.g., agent-based simulations, might generate similar solutions, and the preferred path for generating these solutions needs to be scientifically explored.

Author Contributions: Conceptualization, M.L., R.B. and M.B.; methodology, M.L., R.B. and M.B.; software, M.L.; validation, M.L. and R.B.; formal analysis, M.L.; investigation, M.L.; resources, H.F.; data curation, R.B. and M.B.; writing—original draft preparation, M.L.; writing—review and editing, M.L., R.B. and M.B.; visualization, M.L. and R.B.; supervision, H.F.; project administration, M.L.; funding acquisition, H.F. All authors have read and agreed to the published version of the manuscript.

Funding: The research is part of the project ‘SmartFly’, which is funded by the Saxon State Ministry for Regional Development. It is further part of the project ‘RescueFly’, number 45ILM1016D funded by German Federal Ministry for Digital and Transport. The paper is invited for publication in Future Transportation.

Institutional Review Board Statement: Not applicable.

Informed Consent Statement: Not applicable.

Data Availability Statement: Restrictions apply to the availability of these data. Data were obtained during the SmartFly Study and MiD.

Conflicts of Interest: The authors declare no conflicts of interest. The funders had no role in the design of the study; in the collection, analyses, or interpretation of data; in the writing of the manuscript; or in the decision to publish the results.

Appendix A

Appendix A.1

Table A1. Share of trips within specific hours during the day for suburban areas around Dresden (black line in Figure 5).

Day Hour	Relative Share of Trips	
00:00–00:59 a.m.	0	
01:00–01:59 a.m.	0.001	
02:00–02:59 a.m.	0.001	
03:00–03:59 a.m.	0.001	Night flight restriction
04:00–04:59 a.m.	0.0075	
05:00–05:59 a.m.	0.025	

Table A1. Cont.

Day Hour	Relative Share of Trips	
06:00–06:59 a.m.	0.0625	
07:00–07:59 a.m.	0.08	
08:00–08:59 a.m.	0.065	
09:00–09:59 a.m.	0.065	
10:00–10:59 a.m.	0.06	
11:00–11:59 a.m.	0.0535	
12:00–12:59 p.m.	0.06	
01:00–01:59 p.m.	0.0535	
02:00–02:59 p.m.	0.075	
03:00–03:59 p.m.	0.01	Operation time (green area in Figure 5)
04:00–04:59 p.m.	0.09	
05:00–05:59 p.m.	0.075	
06:00–06:59 p.m.	0.05	
07:00–07:59 p.m.	0.025	
08:00–08:59 p.m.	0.0175	
09:00–09:59 p.m.	0.015	
10:00–10:59 p.m.	0.015	Night flight restriction
11:00–11:59 p.m.	0.005	
Total	1.0000	

Table A2. Energy consumption [kWh] per air taxi category and flight segments.

Segments	Vectored Thrust	Lift and Cruise	Multicopter
Hovertaxi	6.04	3.22	0.45
Vertical take-off and Transition (30 s)	15.87	9.38	0.74
Vertical take-off and Transition (45 s)	19.23	11.22	1.10
Vertical take-off and Transition (60 s)	22.59	13.06	1.47
Vertical take-off and Transition (75 s)	25.95	14.90	1.84
Vertical take-off and Transition (90 s)	29.31	16.74	2.21
Transition and vertical landing (30 s)	14.59	8.51	0.28
Transition and vertical landing (30 s)	17.30	9.91	0.42
Transition and vertical landing (30 s)	20.02	11.31	0.55
Transition and vertical landing (30 s)	22.74	12.72	0.69
Transition and vertical landing (30 s)	25.46	14.12	0.83
Groundtaxi	0.10	0.06	0.07

Table A3. Total energy consumption for cruise segment depending on the destinations.

Destination	Distance GCD [m]	Cruise Distance [m]	Cruise Duration [s]	Total Horizontal Duration [s]	Energy Consumption [kWh]
<i>Vectored Thrust</i>					
Kreischa	11,900	6403	89	242	8.15
Moritzburg	12,600	7103	99	251	8.48
Wilsdruff	13,900	8403	117	269	9.09
Radeberg	14,800	9303	129	282	9.51
Ottendorf-Okr.	16,500	11,003	153	306	10.30
Pirna	17,400	11,903	165	318	10.72
Dippoldisw.	17,900	12,403	172	325	10.96
Meißen	22,300	16,803	233	386	13.02
Glashütte	22,400	16,903	235	387	13.07
Altenberg	31,800	26,303	365	518	17.47
Neustadt/S.	33,500	28,003	389	542	18.26
Chemnitz	62,100	56,603	786	939	31.66
Leipzig	99,900	94,403	1,311	1464	49.39

Table A3. Cont.

Destination	Distance GCD [m]	Cruise Distance [m]	Cruise Duration [s]	Total Horizontal Duration [s]	Energy Consumption [kWh]
<i>Lift and Cruise</i>					
Kreischa	11,900	9781	245	350	6.72
Moritzburg	12,600	10,481	262	368	7.05
Wilsdruff	13,900	11,781	295	400	7.67
Radeberg	14,800	12,681	317	423	8.11
Ottendorf-Okr.	16,500	14,381	360	465	8.92
Pirna	17,400	15,281	382	488	9.35
Dippoldisw.	17,900	15,781	395	500	9.59
Meißen	22,300	20,181	505	610	11.70
Glashütte	22,400	20,281	507	613	11.75
Altenberg	31,800	29,681	742	848	16.25
Neustadt/S.	33,500	31,381	785	980	17.07
Chemnitz	62,100	59,981	1500	1605	30.77
Leipzig	99,900	97,781	2445	2550	48.88
<i>Multicopter</i>					
Kreischa	11,900	10,918	455	537	13.16
Moritzburg	12,600	11,618	484	566	13.88
Wilsdruff	13,900	12,918	538	620	15.21
Radeberg	14,800	13,818	576	658	16.13
Ottendorf-Okr.	16,500	15,518	647	728	17.86
Pirna	17,400	16,418	684	766	18.78
Dippoldisw.	17,900	16,918	705	787	19.29
Meißen	22,300	21,318	888	970	23.79
Glashütte	22,400	21,418	892	974	23.89
Altenberg	31,800	30,818	1284	1366	33.50
Neustadt/S.	33,500	32,518	1355	1437	35.24
Chemnitz	62,100	561,118	2547	2628	64.46
Leipzig	99,900	98,918	4122	4203	103.09

References

1. UAM Initiative Cities Community (UIC2). Manifesto on the Multilevel Governance of the Urban Sky. 2020. Available online: <https://civitas.eu/sites/default/files/UIC2> (accessed on 25 July 2023).
2. European Commission (EC). Smart Cities. 2020. Available online: https://commission.europa.eu/eu-regional-and-urban-development/topics/cities-and-urban-development/city-initiatives/smart-cities_en (accessed on 10 January 2024).
3. Agouridas, V.; Biermann, F.; Czaya, A.; Richter, D.; Stemmler, J.; Stęczyński, J.; Witkowska-Konieczny, A.; Metropolia, G.; Kumar, R.; Metropole, T.; et al. Urban Air Mobility and Sustainable Urban Mobility Planning—Practioner Briefing. 12 2021. Available online: . (accessed on 10 January 2024). [CrossRef]
4. Fraske, T. Change Agency and Path Creation toward Future Transport Systems: A Case Study of the Emerging Urban Air Mobility in Germany. 2022. Available online: <http://dx.doi.org/10.13140/RG.2.2.27722.24000> (accessed on 11 January 2024)
5. Brühl, R.; Fricke, H.; Tober, L.A.; Dextl, F.; Markmiller, J.; Walla, N.; Mutz, C.; Erfurt, R.; Fraske, T.; Medeiros, R.M.; et al. SmartFly—Concept for the Intelligent Integration and Economic Use of Air Taxis in Saxony. 2022. Available online: <http://dx.doi.org/10.13140/RG.2.2.24570.98245>(accessedon11January2024)
6. Vallée, D.; Engel, B.; Vogt, W. (Eds.) *Stadtverkehrsplanung Band 1*; Springer: Berlin/Heidelberg, Germany, 2021. [CrossRef]
7. Teodorović, D.; Janić, M. *Transportation Engineering: Theory, Practice, and Modeling*, 2nd ed.; Butterworth-Heinemann: Cambridge, UK, 2022.
8. Gerike, R.; Hubrich, S.; Ließke, F.; Wittig, S.; Wittwer, R. Sonderauswertung “Mobilität in Städten—SrV 2018”: Oberzentren 500.000 und mehr EW, Topografie Flach (“Mobility in Cities—SrV”: Tables for High-Order Cities of 500,000 and More Inhabitants and with Flat Topography for the Year 2018). 2020. Available online: https://www.researchgate.net/publication/340273317_Sonderauswertung_Mobilitat_in_Stadten_-_SrV_2018_Oberzentren_500000_und_mehr_EW_Topografie_flach_Mobility_in_Cities_-_SrV_Tables_for_high_order_cities_of_500000_and_more_inhabitants_and_with_flat_topo (accessed on 11 January 2024).
9. Nobis, C.; Kuhnimhof, T.; Follmer, R.; Bäumer, M. Mobilität in Deutschland—MiD: Zeitreihenbericht 2002–2008–2017. 2019. Available online: https://bmdv.bund.de/SharedDocs/DE/Anlage/G/mid-zeitreihenbericht-2002-2008-2017.pdf?__blob=publicationFile (accessed on 10 January 2024).
10. Kumar, S.P.; Vinay, M.; Joshi, G.J. *Transportation Planning: Principles, Practises and Policies*, 2nd ed.; PHI Learning Private Limited: Delhi, India, 2017.
11. Ben-Akiva, M.E.; Lerman, S.R. *Discrete Choice Analysis: Theory and Application to Travel Demand*; Number 9 in MIT Press Series in Transportation Studies; MIT Press: Cambridge, MA, USA, 1985.

12. Golob, T.F.; Beckmann, M.J.; Zahavi, Y. A utility-theory travel demand model incorporating travel budgets. *Transp. Res. Part Methodol.* **1981**, *15*, 375–389. [[CrossRef](#)]
13. Sun, X.; Wandelt, S.; Husemann, M.; Stumpf, E. Operational Considerations regarding On-Demand Air Mobility: A Literature Review and Research Challenges. *J. Adv. Transp.* **2021**, *2021*, 3591034. [[CrossRef](#)]
14. Balac, M. The market potential of Urban Air Mobility in the USA: Analysis based on open-data. In Proceedings of the 2021 IEEE International Intelligent Transportation Systems Conference (ITSC), Indianapolis, IN, USA, 19–22 September 2021; pp. 1419–1424. [[CrossRef](#)]
15. Justin, C.Y.; Payan, A.P.; Mavris, D. Demand modeling and operations optimization for advanced regional air mobility. In Proceedings of the AIAA AVIATION 2021 FORUM, Virtual Event, 2–6 August 2021; p. 3179. [[CrossRef](#)]
16. Rajendran, S.; Srinivas, S.; Grimshaw, T. Predicting demand for air taxi urban aviation services using machine learning algorithms. *J. Air Transp. Manag.* **2021**, *92*, 102043. [[CrossRef](#)]
17. Wu, Z.; Zhang, Y. Integrated Network Design and Demand Forecast for On-Demand Urban Air Mobility. *Engineering* **2021**, *7*, 473–487. [[CrossRef](#)]
18. Bulusu, V.; Onat, E.B.; Sengupta, R.; Yedavalli, P.; Macfarlane, J. A traffic demand analysis method for urban air mobility. *IEEE Trans. Intell. Transp. Syst.* **2021**, *22*, 6039–6047. [[CrossRef](#)]
19. Yedavalli, P.S.; Onat, E.; Peng, X.; Sengupta, R.; Waddell, P.; Bulusu, V.; Xue, M. Assessing the Value of Urban Air Mobility through Metropolitan-Scale Microsimulation: A Case Study of the San Francisco Bay Area. In Proceedings of the AIAA AVIATION 2021 FORUM, Virtual Event, 2–6 August 2021; p. 2338. [[CrossRef](#)]
20. Rothfeld, R.; Fu, M.; Balać, M.; Antoniou, C. Potential urban air mobility travel time savings: An exploratory analysis of Munich, Paris, and San Francisco. *Sustainability* **2021**, *13*, 2217. [[CrossRef](#)]
21. Park, B.T.; Kim, H.; Kim, S.H. Vertiport Performance Analysis for On-Demand Urban Air Mobility Operation in Seoul Metropolitan Area. *Int. J. Aeronaut. Space Sci.* **2022**, *23*, 1065–1078. [[CrossRef](#)]
22. Jeong, J.; So, M.; Hwang, H.Y. Selection of Vertiports Using K-Means Algorithm and Noise Analyses for Urban Air Mobility (UAM) in the Seoul Metropolitan Area. *Appl. Sci.* **2021**, *11*, 5729. [[CrossRef](#)]
23. Peksa, M.; Bogenberger, K. Estimating UAM Network Load with Traffic Data for Munich. In Proceedings of the 2020 AIAA/IEEE 39th Digital Avionics Systems Conference (DASC), San Antonio, TX, USA, 11–15 October 2020; pp. 1–7. [[CrossRef](#)]
24. Fu, M.; Straubinger, A.; Schaumeier, J. Scenario-based Demand Assessment of Urban Air Mobility in the Greater Munich Area. *J. Air Transp.* **2022**, *30*, 125–136. [[CrossRef](#)]
25. Balac, M.; Rothfeld, R.L.; Hörl, S. The prospects of on-demand urban air mobility in Zurich, Switzerland. In Proceedings of the 2019 IEEE Intelligent Transportation Systems Conference (ITSC), Auckland, New Zealand, 27–30 October, 2019; pp. 906–913. [[CrossRef](#)]
26. Finkeldei, W.; Feldhoff, E.; Roque, G.S. *Flughafen Köln/Bonn Flugtaxi Infrastruktur: Machbarkeitsstudie*; Flughafen Köln/Bonn GmbH: Cologne, Germany, 2020. (In Germany)
27. Götz, K.; Deffner, J.; Klinger, T. Mobilitätsstile und Mobilitätskulturen—Erklärungspotentiale, Rezeption und Kritik. In *Handbuch Verkehrspolitik*; Springer: Wiesbaden, Germany, 2016; pp. 781–804. [[CrossRef](#)]
28. Batty, P.; Palacin, R.; González-Gil, A. Challenges and opportunities in developing urban modal shift. *Travel Behav. Soc.* **2015**, *2*, 109–123. [[CrossRef](#)]
29. Riza, L.; Bruehl, R.; Fricke, H.; Planing, P. Will air taxis extend public transportation? A scenario-based approach on user acceptance in different urban settings. *Transp. Res. Interdiscip. Perspect.* **2024**, *23*, 101001. [[CrossRef](#)]
30. Straubinger, A.; Rothfeld, R.; Shamiyeh, M.; Büchter, K.D.; Kaiser, J.; Plötner, K.O. An overview of current research and developments in urban air mobility—Setting the scene for UAM introduction. *J. Air Transp. Manag.* **2020**, *87*, 101852. [[CrossRef](#)]
31. Brühl, R.; Fricke, H.; Schultz, M. Air taxi flight performance modeling and application. In Proceedings of the ATM Seminar, Virtual, 20–24 September 2021.
32. Lee, B.S.; Yun, J.Y.; Hwang, H.Y. Flight Range and Time Analysis for Classification of eVTOL PAV. *J. Adv. Navig. Technol.* **2020**, *24*, 73–84. [[CrossRef](#)]
33. Bacchini, A.; Cestino, E. Electric VTOL configurations comparison. *Aerospace* **2019**, *6*, 26. [[CrossRef](#)]
34. Rajendran, S.; Zack, J. Insights on strategic air taxi network infrastructure locations using an iterative constrained clustering approach. *Transp. Res. Part E Logist. Transp. Rev.* **2019**, *128*, 470–505. [[CrossRef](#)]
35. The Vertical Flight Society. eVTOL Aircraft Directory. 2022. Available online: <https://evtol.news/aircraft> (accessed on 10 January 2024).
36. Datta, A.; Elbers, S.; Wakayama, S.; Alonso, J.; Botero, E.; Carter, C.; Martins, F. Commercial Intra-City On-Demand Electric-VTOL Status of Technology. AHS/NARI Transformative Vertical Flight Working Group-2; 2018. Available online: <https://vtol.org/files/dmfile/TVF.WG2.YR2017draft.pdf> (accessed on 11 January 2024).
37. Miao, Y.; Hynan, P.; von Jouanne, A.; Yokochi, A. Current Li-Ion Battery Technologies in Electric Vehicles and Opportunities for Advancements. *Energies* **2019**, *12*, 1074. [[CrossRef](#)]
38. Cadex Electronics. BU-216: Summary Table of Lithium-Based Batteries. 2020. Available online: <https://batteryuniversity.com/article/bu-216-summary-table-of-lithium-based-batteries> (accessed on 10 January 2024).

39. International Civil Aviation Organisation (ICAO). Procedures for Air Navigation Services (PANS) Aircraft Operations (OPS). 2018. Available online: <https://fac.ch/wp-content/uploads/2020/11/ICAO-Doc-8168-Volume-III-Aircraft-Operating-Procedures.pdf> (accessed on 11 January 2024).
40. Shamiyeh, M.; Rothfeld, R.; Hornung, M. A performance benchmark of recent personal air vehicle concepts for urban air mobility. In Proceedings of the 31st Congress of the International Council of the Aeronautical Sciences, Belo Horizonte, Brazil, 9–14 September 2018.
41. UBER Elevate. Uber Air Vehicle Requirements and Missions. 2018. Available online: <https://s3.amazonaws.com/uber-static/elevate/Summary+Mission+and+Requirements.pdf> (accessed on 11 January 2024).
42. Brühl, R.; Fricke, H. Assessment of minimum ground time for air taxis based on turnaround critical path modeling. In Proceedings of the 10th Edition of the International Conference on Research in Air Transportation (ICRAT), Tampa, FL, USA, 19–23 June 2022.
43. Beamon, B.M.; Chen, V.C.P. Performability-based fleet sizing in a material handling system. *Int. J. Adv. Manuf. Technol.* **1998**, *14*, 441–449. [[CrossRef](#)]
44. Imen, L.; Wassim, M.; Mounir, E.; Hedi, C. Improvement opportunities of a Simulation/Expert System Approach for Manufacturing System Sizing: A review and proposal. *Adv. Sci. Technol. Eng. Syst. J.* **2019**, *4*, 213–223. [[CrossRef](#)]
45. Ehlers, S.; Pache, H.; von Bock und Polach, F.; Johnsen, T. A Fleet Efficiency Factor for fleet size and mix problems using particle swarm optimisation. *Ship Technol. Res.* **2019**, *66*, 106–116. [[CrossRef](#)]
46. Cheng, L.; Wang, K.; De Vos, J.; Huang, J.; Witlox, F. Exploring non-linear built environment effects on the integration of free-floating bike-share and urban rail transport: A quantile regression approach. *Transp. Res. Part A Policy Pract.* **2022**, *162*, 175–187. [[CrossRef](#)]
47. Guidon, S.; Reck, D.J.; Axhausen, K. Expanding a (n)(electric) bicycle-sharing system to a new city: Prediction of demand with spatial regression and random forests. *J. Transp. Geogr.* **2020**, *84*, 102692. [[CrossRef](#)]
48. Kania, M.; Assmann, T. Data-Driven Approach for Defining Demand Scenarios for Shared Autonomous Cargo-Bike Fleets. In *Smart Energy for Smart Transport: Proceedings of the 6th Conference on Sustainable Urban Mobility, CSUM2022, Skiathos Island, Greece, 31 August–2 September 2022*; Springer: Berlin/Heidelberg, Germany, 2023; pp. 1374–1405. [[CrossRef](#)]
49. Hua, M.; Chen, X.; Chen, J.; Jiang, Y. Minimizing fleet size and improving vehicle allocation of shared mobility under future uncertainty: A case study of bike sharing. *J. Clean. Prod.* **2022**, *370*, 133434. [[CrossRef](#)]
50. Wittmann, M.; Neuner, L.; Lienkamp, M. A Predictive Fleet Management Strategy for On-Demand Mobility Services: A Case Study in Munich. *Electronics* **2020**, *9*, 1021. [[CrossRef](#)]
51. Ye, X.; Li, M.; Yang, Z.; Yan, X.; Chen, J. A dynamic adjustment model of cruising taxicab fleet size combined the operating and flied survey data. *Sustainability* **2020**, *12*, 2776. [[CrossRef](#)]
52. Ko, S.; Lautala, P.; Zhang, K. Data-Driven Study on the Sustainable Log Movements: Impact of Rail Car Fleet Size on Freight Storage and Car Idling. *Sustainability* **2020**, *12*, 4563. [[CrossRef](#)]
53. Csereklyei, Z.; Stern, D.I. Flying more efficiently: Joint impacts of fuel prices, capital costs and fleet size on airline fleet fuel economy. *Ecol. Econ.* **2020**, *175*, 106714. [[CrossRef](#)]
54. Müller, C.; Kieckhäfer, K.; Spengler, T.S. The influence of emission thresholds and retrofit options on airline fleet planning: An optimization approach. *Energy Policy* **2018**, *112*, 242–257. [[CrossRef](#)]
55. Mohri, S.S.; Nasrollahi, M.; Pirayesh, A.; Mohammadi, M. An integrated global airline hub network design with fleet planning. *Comput. Ind. Eng.* **2022**, *164*, 107883. [[CrossRef](#)]
56. Liu, M.; Ding, Y.; Sun, L.; Zhang, R.; Dong, Y.; Zhao, Z.; Wang, Y.; Liu, C. Green Airline-Fleet Assignment with Uncertain Passenger Demand and Fuel Price. *Sustainability* **2023**, *15*, 899. [[CrossRef](#)]
57. Agrawal, P.; Pravinovngvuth, S. Estimation of Travel Demand for Bangkok; Chiang Mai Hyperloop Using Traveler Surveys. *Sustainability* **2021**, *13*, 14037. [[CrossRef](#)]
58. Sha, M.; Srinivasan, R. Fleet sizing in chemical supply chains using agent-based simulation. *Comput. Chem. Eng.* **2016**, *84*, 180–198. [[CrossRef](#)]
59. Samchuk, G.; Kopytkov, D.; Rossolov, A. Freight Fleet Management Problem: Evaluation of a Truck Utilization Rate Based on Agent Modeling. *Commun.-Sci. Lett. Univ. Zilina* **2022**, *24*, D46–D58. [[CrossRef](#)]
60. Valmiki, P.; Reddy, A.S.; Panchakarla, G.; Kumar, K.; Purohit, R.; Suhane, A. A study on simulation methods for AGV fleet size estimation in a flexible manufacturing system. *Mater. Today Proc.* **2018**, *5*, 3994–3999. [[CrossRef](#)]
61. Saprykin, A.; Chokani, N.; Abhari, R.S. Impacts of downscaled inputs on the predicted performance of taxi fleets in agent-based scenarios including Mobility-as-a-Service. *Procedia Comput. Sci.* **2022**, *201*, 574–580. [[CrossRef](#)]
62. Rajendran, S.; Shulman, J. Study of emerging air taxi network operation using discrete-event systems simulation approach. *J. Air Transp. Manag.* **2020**, *87*, 101857. [[CrossRef](#)]
63. Papier, F.; Thonemann, U.W. Queuing Models for Sizing and Structuring Rental Fleets. *Transp. Sci.* **2008**, *42*, 302–317. . [[CrossRef](#)]
64. Fantì, M.P.; Mangini, A.M.; Pedroncelli, G.; Ukovich, W. Fleet sizing for electric car sharing system via closed queueing networks. In Proceedings of the 2014 IEEE International Conference on Systems, Man, and Cybernetics (SMC), San Diego, CA, USA, 5–8 October 2014; pp. 1324–1329. [[CrossRef](#)]

65. Amjath, M.; Kerbache, L.; Smith, J.M.; Elomri, A. Fleet sizing of trucks for an inter-facility material handling system using closed queueing networks. *Oper. Res. Perspect.* **2022**, *9*, 100245. [[CrossRef](#)]
66. Golden, B.; Assad, A.; Levy, L.; Gheysens, F. The fleet size and mix vehicle routing problem. *Comput. Oper. Res.* **1984**, *11*, 49–66. [[CrossRef](#)]
67. Vis, I.F.; de Koster, R.M.B.; Savelsbergh, M.W. Minimum vehicle fleet size under time-window constraints at a container terminal. *Transp. Sci.* **2005**, *39*, 249–260. [[CrossRef](#)]
68. Li, Z.; Tao, F. On determining optimal fleet size and vehicle transfer policy for a car rental company. *Comput. Oper. Res.* **2010**, *37*, 341–350. [[CrossRef](#)]
69. Repoussis, P.; Tarantilis, C. Solving the Fleet Size and Mix Vehicle Routing Problem with Time Windows via Adaptive Memory Programming. *Transp. Res. Part C Emerg. Technol.* **2010**, *18*, 695–712. [[CrossRef](#)]
70. Çağrı Koç.; Bektaş, T.; Jabali, O.; Laporte, G. The fleet size and mix location-routing problem with time windows: Formulations and a heuristic algorithm. *Eur. J. Oper. Res.* **2016**, *248*, 33–51. [[CrossRef](#)]
71. Jara-Díaz, S.; Fielbaum, A.; Gschwender, A. Optimal fleet size, frequencies and vehicle capacities considering peak and off-peak periods in public transport. *Transp. Res. Part A Policy Pract.* **2017**, *106*, 65–74. [[CrossRef](#)]
72. Dresdner Verkehrsbetriebe, A.G.; Landeshauptstadt Dresden, V. Traditionen, Trips & Trends—Mobilität in Dresden und Umland unter der Lupe - Ergebnisse aus der Verkehrserhebung SrV [German], 2018. Available online: https://www.dresden.de/media/pdf/stadtplanung/verkehr/SrV_2018_Broschuere.pdf (accessed on 11 January 2024).
73. Gesellschaft für Luftverkehrsforschung (GfL). *Bereitstellung Lokaler Mobilitätsparameter und Mobilitätseigenschaften für Lufttaxis auf Basis Bundesweiter Daten Gemäß den Befragungen "Mobilität in Deutschland" und "Verkehr in Städten"* [German]; Gesellschaft für Luftverkehrsforschung (GfL): Dresden, Germany, 2022.
74. Brühl, R.; Fricke, H. Locating air taxi infrastructure in regional areas—The Saxony use case. In Proceedings of the Deutscher Luft- und Raumfahrtkongress (DLRK) 2022, Dresden, Germany, 29 September 2022.
75. Krueger, R.; Rashidi, T.H.; Rose, J.M. Preferences for shared autonomous vehicles. *Transp. Res. Part C Emerg. Technol.* **2016**, *69*, 343–355. [[CrossRef](#)]
76. Fu, M.; Rothfeld, R.; Antoniou, C. Exploring preferences for transportation modes in an urban air mobility environment: Munich case study. *Transp. Res. Rec.* **2019**, *2673*, 427–442. [[CrossRef](#)]
77. Thompson, M. Panel: Perspectives on prospective markets. In Proceedings of the 5th Annual AHS Transformative VTOL Workshop, San Francisco, CA, USA, 18–19 January 2018; pp. 18–19.
78. Shaheen, S.; Cohen, A.; Farrar, E. The Potential Societal Barriers of Urban Air Mobility (UAM). 2018. Available online: <http://dx.doi.org/10.7922/G28C9TFR>(accessedon11January2024)
79. Statistisches Landesamt des Freistaates Sachsen. Bevölkerungsstand, Einwohnerzahlen. 2021. Available online: <https://www.statistik.sachsen.de/html/bevoelkerungsstand-einwohner.html> (accessed on 10 January 2024).
80. Statistische Ämter der Länder. Pendleratlas Deutschland. 2023. Available online: <https://pendleratlas.statistikportal.de/> (accessed on 10 January 2024).
81. Johnson, W. *Helicopter Theory*; Princeton University Press: Princeton, NJ, USA, 1980.
82. van der Wall, B.G. *Grundlagen der Hubschrauber-Aerodynamik (German)*; Springer: Berlin/Heidelberg, Germany, 2020.
83. Kamal, A.M.; Ramirez-Serrano, A. Design methodology for hybrid (VTOL + Fixed Wing) unmanned aerial vehicles. *Aeronaut. Aerosp. Open Access J.* **2018**, *2*, 165–176 [[CrossRef](#)]
84. Patterson, M.; Antcliff, K.; Kohlman, L. A proposed Approach to Studying Urban Air Mobility Missions including an Initial Exploration of Mission Requirements. In Proceedings of the AHS International 74th Annual Forum & Technology Display, Phoenix, AZ, USA, 15–17 May 2018.
85. Rosenow, J.; Zeh, T.; Lindner, M.; Förster, S.; Fricke, H.; Caraud, A. Multiple Aircraft in a multi-criteria Trajectory Optimization. In Proceedings of the Fifteenth USA/Europe Air Traffic Management Research and Development Seminar (ATM2023), Savannah, GA, USA, 5–9 June 2023.
86. Sun, J.; Ellerbroek, J.; Hoekstra, J. Modeling aircraft performance parameters with open ADS-B data. In Proceedings of the 12th USA/Europe Air Traffic Management Research and Development Seminar, Seattle, WA, USA, 27–30 June 2017.
87. Hepperle, M. Electric Flight—Potential and Limitations. In Proceedings of the AVT-209 Workshop on Energy Efficient Technologies and Concepts of Operation, Lisbon, Portugal, 22–24 October 2012.
88. Evler, J.; Lindner, M.; Fricke, H.; Schultz, M. Integration of turnaround and aircraft recovery to mitigate delay propagation in airline networks. *Comput. Oper. Res.* **2022**, *138*, 105602. [[CrossRef](#)]
89. Lindner, M.; Fricke, H. Performance Degradation based Aircraft Tail Assignment and Routing in Daily Airline Operations. In Proceedings of Deutscher Luft- und Raumfahrtkongress DLRK 2022, Dresden, Germany, 27–29 September 2022.
90. De Smet, G.; Open Source Contributors. *OptaPlanner User Guide*; Red Hat, Inc. or Third-Party Contributors, 2006; OptaPlanner is an Open Source Constraint Solver in Java. Available online: https://docs.optaplanner.org/latest/optaplanner-docs/html_single/index.html (accessed on 25 July 2023).

-
91. De Neufville, R. Airport systems planning, design, and management. In *Air Transport Management*; Routledge: Abingdon, UK, 2020; pp. 79–96.
 92. Chen, L.; Wandelt, S.; Dai, W.; Sun, X. Scalable Vertiport Hub Location Selection for Air Taxi Operations in a Metropolitan Region. *INFORMS J. Comput.* **2022**, *34*, 834–856. [[CrossRef](#)]

Disclaimer/Publisher’s Note: The statements, opinions and data contained in all publications are solely those of the individual author(s) and contributor(s) and not of MDPI and/or the editor(s). MDPI and/or the editor(s) disclaim responsibility for any injury to people or property resulting from any ideas, methods, instructions or products referred to in the content.